

# Selective Polycarboxylation of Semiconducting Single-Walled Carbon Nanotubes by Reductive Sidewall Functionalization

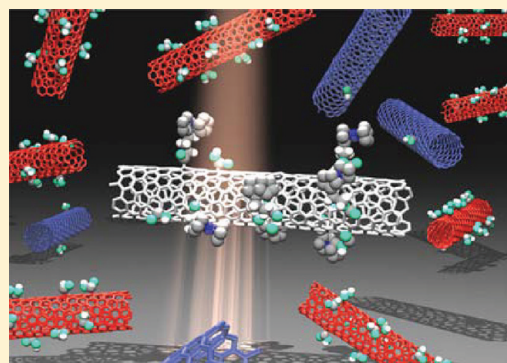
Benjamin Gebhardt,<sup>†</sup> Ferdinand Hof,<sup>†</sup> Claudia Backes,<sup>†</sup> Matthias Müller,<sup>‡</sup> Thomas Plocke,<sup>‡</sup> Janina Maultzsch,<sup>‡</sup> Christian Thomsen,<sup>‡</sup> Frank Hauke,<sup>†</sup> and Andreas Hirsch<sup>\*†</sup>

<sup>†</sup>Department of Chemistry and Pharmacy & Institute of Advanced Materials and Processes (ZMP), University of Erlangen-Nuremberg, Henkestrasse 42, 91054 Erlangen, Germany

<sup>‡</sup>Institute of Solid State Physics, Technical University Berlin, Hardenbergstrasse 36, 10623 Berlin, Germany

Supporting Information

**ABSTRACT:** The efficient and controllable synthesis, the detailed characterization, and the chemical postfunctionalization of polycarboxylated single-walled carbon nanotubes SWCNT(COOH)<sub>n</sub> are reported. This innovative covalent sidewall functionalization method is characterized by (a) the preservation of the integrity of the entire  $\sigma$ -framework of SWCNTs; (b) the possibility of achieving very high degrees of addition; (c) control of the functionalization degrees by the variation of the reaction conditions (reaction time, ultrasonic treatment, pressure); (d) the identification of conditions for the selective functionalization of semiconducting carbon nanotubes, leaving unfunctionalized metallic tubes behind; (e) the proof that the introduced carboxylic acid functionalities can serve as versatile anchor points for the coupling to functional molecules; and (f) the application of a subsequent thermal degradation step of the functionalized semiconducting tubes leaving behind intact metallic SWCNTs. Functional derivatives have been characterized in detail by means of Raman, UV-vis/nIR, IR, and fluorescence spectroscopy as well as by thermogravimetric analysis combined with mass spectrometry, atomic force microscopy, and zeta-potential measurements.



## ■ INTRODUCTION

The outstanding mechanical and electronic properties of single-walled carbon nanotubes (SWCNTs) challenge the development of practical applications of this family of synthetic carbon allotropes.<sup>1–8</sup> However, for their implementation in high performance components, a number of substantial hurdles have still to be overcome. First, the limited solubility<sup>9–12</sup> of SWCNTs in water or common organic solvents has to be increased dramatically to facilitate the processing of this novel carbon allotrope. Second, highly selective, efficient, and tunable functionalization protocols remain to be rare, although they are required for a tailored design of the tube properties and their combination with other compound classes.<sup>13–16</sup> Third, efficient and high yield separation procedures for both metallic and semiconducting tubes have to be elaborated to pave the road for electronic applications.<sup>17–19</sup> Covalent chemical functionalization of the carbon framework of SWCNTs is a promising tool for overcoming these three major obstacles.<sup>7,14,20–23</sup>

The introduction of carboxylic acid functionalities to the nanotube scaffold by oxidation procedures was one first step into this direction and gave access to a considerably increased solubility of the respective SWCNT derivatives and provided anchor points for subsequent defect functionalization-based coupling reactions<sup>24–26</sup> with polymers, proteins, nanoparticles, donor–acceptor systems, and so forth. Nevertheless, a

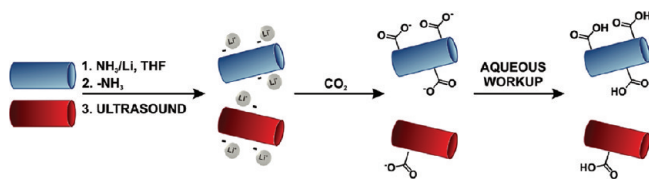
fundamental drawback of this approach is the fact that during the oxidation procedures, a large portion of the SWCNTs is destroyed or considerably shortened. Moreover, the introduction of the respective carboxylic groups at the surface of the tubes is inevitably accompanied by the impossibility of healing the generated holes in the tube sidewalls, as  $\sigma$ -bonds of the nanotube scaffold have been broken under these oxidative conditions. In other words, all of the carboxylic C-atoms originate from former  $sp^2$ -C-atoms of the sidewall framework. Therefore, these dramatic damages of the  $sp^2$ -carbon network are accompanied by the loss of many of the characteristic and unprecedented tube properties.

Conceptually, the introduction of carboxylic acid functionalities without destroying the SWCNT  $\sigma$ -framework could be accomplished by an electrophilic addition of CO<sub>2</sub> to intermediately reduced nanotubes. Unfortunately, early attempts into this direction, such as the subsequent addition of sec-butyl lithium and carbon dioxide reported by Chen et al.,<sup>27</sup> led only to very low degrees of sidewall functionalization. In other approaches, the introduction of alkyl spacers has been pursued,<sup>28,29</sup> resulting in no direct binding of the carboxylic acid groups to the nanotube  $\pi$ -system.

Received: July 21, 2011

Published: October 27, 2011

**Scheme 1. Preferred Reductive Polycarboxylation of Semiconducting SWCNTs under Modified Birch Conditions: Blue, Semiconducting; Red, Metallic SWCNTs**



With respect to the third hurdle pointed out above, SWCNT sorting, an appealing concept for a SWCNT separation would be the selective binding of addends to either metallic or semiconducting species in the course of a covalent sidewall functionalization procedure. During past years, research groups all over the world elaborated a small portfolio of selective sidewall functionalization sequences such as, for example, the addition of diazonium compounds,<sup>30–32</sup> the reductive alkylation,<sup>33</sup> and the nucleophilic attack of organometallic reagents,<sup>34,35</sup> which invariably prefer metallic carbon nanotubes over semiconducting nanotubes. However, no electronic type selective functionalization sequence toward semiconducting SWCNT species has been elaborated to the present. To complete the picture and to address all three major impediments at once, an ultimate reaction sequence for carbon nanotubes is still missing, up to now.

Herein, we present a SWCNT sidewall carboxylation reaction based on ubiquitarily available carbon dioxide, which is characterized by (a) a direct covalent coupling of carboxylic acid functionalities to the intact  $\sigma$ -framework of SWCNT sidewalls; (b) the possibility of achieving very high degrees of addition; (c) the control of the degree of functionalization by the variation of different reaction conditions (reaction time, ultrasonic treatment, pressure); (d) the identification of conditions for the selective functionalization of semiconducting carbon nanotubes, leaving unfunctionalized metallic tubes behind; (e) the proof that the introduced carboxylic acid functionalities can serve as versatile anchor points for the coupling to functional molecules; and (f) the application of a subsequent thermal degradation step of the functionalized semiconducting tubes leaving behind intact metallic SWCNTs. These discoveries pave the way for applying the entire chemistry of carboxylic acid group based coupling reactions with functional molecules to generate new families of covalently functionalized SWCNT derivatives with preserved structural and electronic properties.<sup>36–39</sup> Moreover, the bulk separation of metallic and semiconducting tube species can be carried out on the basis of this selective addition of carbon dioxide to semiconducting species, which has not been observed before.

## RESULTS AND DISCUSSION

**Synthesis.** Our approach to sidewall carboxylated carbon nanotubes  $\text{SWCNT}(\text{COOH})_n$ , presented in this contribution is based on the idea of trapping reduced  $\text{SWCNT}^{n-}$  intermediates with gaseous  $\text{CO}_2$  serving as an electrophilic trapping molecule. The concept is related to the reductive alkylation of carbon nanotubes introduced by Billups et al.,<sup>40–42</sup> where SWCNTs were reduced with lithium metal in liquid ammonia and subsequently quenched with alkyl or aryl iodides as electrophiles. However, this original protocol is not suitable for a trapping reaction with carbon dioxide as liquid ammonia represents a

highly reactive environment. Molecules sensitive to such harsh reaction conditions cannot be applied for SWCNT sidewall derivatization sequences. Therefore, we modified the reaction sequence (Scheme 1) by the substitution of ammonia with THF as solvent<sup>43</sup> (for detailed experimental conditions, see the Experimental Section). These modifications allowed for a most efficient polycarboxylation of SWCNTs. As will be pointed out below, this reaction sequence is, at the same time, highly selective toward a preferred functionalization of semiconducting versus metallic nanotubes. In a typical protocol, SWCNTs were dispersed by ultrasound agitation in dry THF. The reductive conditions were then established by condensing liquid ammonia into the reaction medium followed by the addition of lithium metal. Afterward, the ammonia was evaporated and the remaining lithium bronze was removed, yielding a stable black THF dispersion of the reduced tubes ( $\text{SWCNT}^{n-}$ ). After this procedure, no solvated electrons remain.<sup>43</sup> In some cases, such dispersions were then repeatedly ultrasonicated to optimize exfoliation and individualization of the negatively charged nanotube intermediates.

As will be outlined below, the second ultrasonication step is a fundamental prerequisite for the selectivity of the  $\text{CO}_2$  binding. After aqueous workup, the polycarboxylated tubes  $\text{SWCNT}-(\text{COOH})_n$  were obtained as final reaction products. As carbon dioxide source, either solid dry ice or gaseous  $\text{CO}_2$  was used. In analogy to the reactions with alkyl and aryl iodides investigated by Billups et al.,<sup>44,45</sup> a single electron transfer (SET) from the  $\text{SWCNT}^{n-}$  intermediates to  $\text{CO}_2$  as initial reaction step is suggested. The resulting radical anion  $\text{CO}_2^{\cdot-}$  can subsequently attack the SWCNT surface in the sense of a radical addition to the unsaturated  $\pi$ -system of the nanotube scaffold. As compared to these optimized reaction conditions, the treatment of reduced tubes in liquid ammonia with  $\text{CO}_2$  in the presence of excess alkaline metal (conventional Birch conditions) leads only to very low functionalization degrees in the products ( $\text{SWCNT}-(\text{COOH})_n$  (Birch) (1)) and, moreover, to the formation of large amounts of white side products generated from the reductive conversion of carbon dioxide.

The polycarboxylated tubes prepared via our modified reaction conditions without a second ultrasonication step are denoted as  $\text{SWCNT}(\text{COOH})_n$  (THF) (2). Polycarboxylated SWCNT derivatives prepared with an additional ultrasonication step directly before the carboxylation are labeled as  $\text{SWCNT}-(\text{COOH})_n$  (THF/ultrasound) (3) when the HiPCO tube batch P035S was used for the functionalization and denoted as  $\text{SWCNT}(\text{COOH})_n$  (THF/ultrasound) (4) with HiPCO tube batch P0261 as starting material. For a further increase of the degree of functionalization, the reactions were also performed under high  $\text{CO}_2$  pressures of 33 and 55 bar in an autoclave, respectively. Therefore, the corresponding reaction products are denoted as  $\text{SWCNT}(\text{COOH})_n$  (THF/ultrasound/30 bar) (5) and  $\text{SWCNT}(\text{COOH})_n$  (THF/ultrasound/55 bar) (6).

**Raman Spectroscopy.** The direct sidewall carboxylation of the SWCNTs is clearly reflected by characteristic changes in the respective Raman spectra of the carbon allotrope. This characterization technique has been established as the primary tool for the investigation of the covalent sidewall functionalization of SWCNTs.<sup>46–50</sup> The covalent attachment of addends is accompanied by the introduction of  $\text{sp}^3$ -defects, which has a direct impact on the intensity of certain Raman bands. The most prominent spectral change constitutes an increase of the intensity of the defect induced D-band ( $\sim 1300 \text{ cm}^{-1}$ ) based on a

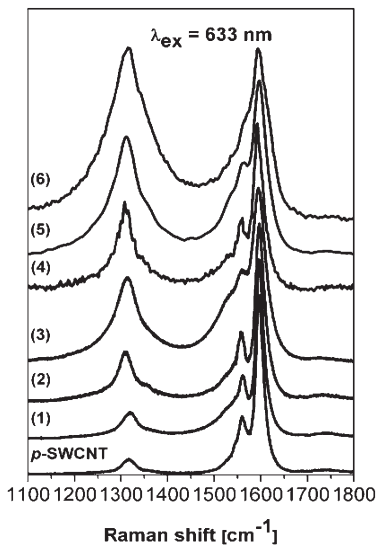


**Figure 1.** D- and G-band regions of the Raman spectra of sidewall carboxylated SWCNT(COOH)<sub>n</sub> (**1–6**). Excitation wavelength 633 nm. Spectra offset for clarity.

**Table 1. Normalized  $A_D/A_G$  Values Obtained from the Raman Spectra (633 nm Excitation) of SWCNT(COOH)<sub>n</sub> (**1–6**)<sup>a</sup>**

	$A_D/A_G$ 633 nm
(6) SWCNT(COOH) <sub>n</sub> (THF/ultrasound/55 bar)	21.7
(5) SWCNT(COOH) <sub>n</sub> (THF/ultrasound/30 bar)	11.3
(4) SWCNT(COOH) <sub>n</sub> (THF/ultrasound)	9.3
(3) SWCNT(COOH) <sub>n</sub> (THF/ultrasound)	5.1
(2) SWCNT(COOH) <sub>n</sub> (THF)	4.9
(1) SWCNT(COOH) <sub>n</sub> (Birch)	2.3
p-SWCNT	1.0

<sup>a</sup> The normalized values are defined as  $A_D/A_G = (A_{D\text{sample}}/A_{G\text{sample}})/(A_{D0}/A_{G0})$ .  $A_{D0}$  and  $A_{G0}$  are the areas for the respective starting material (p-SWCNT).

rehybridization of  $\text{sp}^2$  lattice carbon atoms into  $\text{sp}^3$  configuration. Accordingly, the normalized area ratio of the D-band to the G-band ( $\sim 1590 \text{ cm}^{-1}$ ) ( $A_D/A_G$ ) with respect to the ratio of the as-received starting material ( $A_{D0}/A_{G0}$ ) can be regarded as a good measure for the degree of functionalization. The resonant Raman spectra obtained with an excitation wavelength of 633 nm impressively illustrate this increase in the D-band intensity (Figure 1) for the functionalized SWCNT derivatives (spectral data for 532 and 785 nm excitation are presented in the Supporting Information: Figure S1, S2 (532 nm) and Figure S3, S4 (785 nm)). As is clearly discernible, the functionalized nanotubes SWCNT(COOH)<sub>n</sub> (Birch) (**1**) obtained upon  $\text{CO}_2$  addition of conventionally Birch reduced tubes exhibit a very low degree of functionalization, which is expressed by a  $A_D/A_G$  value of only 2.3. In contrast, under modified reduction conditions, a pronounced increase of the  $\text{sp}^3$ -defect induced Raman D-band can be detected even without the second ultrasonic agitation, yielding the respective SWCNT polycarboxylates SWCNT(COOH)<sub>n</sub> (THF) (**2**); the corresponding  $A_D/A_G$  ratio increases considerably to 4.9. In the case of a second ultrasonic agitation of the THF solution containing the reduced SWCNT<sup>n-</sup> species, the degree of functionalization can be further increased to a  $A_D/A_G$  value

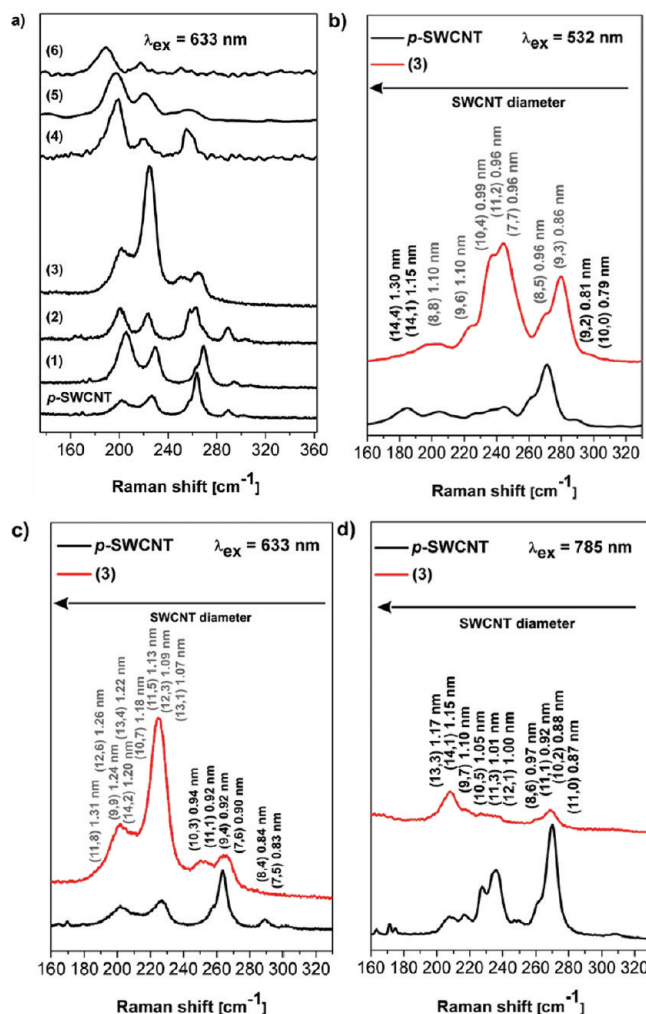


**Figure 2.** (a) RBM region (633 nm excitation wavelength) of sidewall carboxylated SWCNTs (**1–6**). (b–d) Comparison of the RBM bands of SWCNT(COOH)<sub>n</sub> (THF/ultrasound) (**3**) with the corresponding Raman signals of the starting material (p-SWCNT) recorded at three different excitation wavelengths: 532, 633, and 785 nm, respectively.

of 5.6 for SWCNT(COOH)<sub>n</sub> (THF/ultrasound) (**3**) and 9.3 for SWCNT(COOH)<sub>n</sub> (THF/ultrasound) (**4**), respectively. The highest degrees of functionalization are obtained when the additional high pressure conditions are applied. For SWCNT(COOH)<sub>n</sub> (THF/ultrasound/30 bar) (**5**) and SWCNT(COOH)<sub>n</sub> (THF/ultrasound/50 bar) (**6**), the  $A_D/A_G$  ratios reach 11.3 and 21.7, respectively. This demonstrates a clear pressure dependence of the underlying polycarboxylation reaction, and it also shows nicely that the degree of functionalization can easily be controlled (Table 1). This influence of the pressure is indicative of a reversible  $\text{CO}_2$  binding to the negatively charged SWCNT intermediates, in analogy to our previous investigations on the nucleophilic addition of metal alkylides and metal amides.<sup>51</sup> However, once the overall reaction sequence is completed and the reaction products SWCNT(COOH)<sub>n</sub> without additional charges on the sidewall have been isolated, no  $\text{CO}_2$  release under ambient conditions is observed.

Another significant result of the Raman studies is the fact that the increase of the intensities of the defect induced D-bands of semiconducting tubes is much more pronounced than those of

the metallic tubes, especially for the products 3–6 prepared with the additional second ultrasonication step of the intermediates  $\text{SWCNT}^{n-}$  (Figures S1 and S3). This is a clear indication for the preferred functionalization of semiconducting tubes. In particular at 785 nm, where predominantly semiconducting tubes are in resonance, the D-band is substantially increased up to  $A_{\text{D}}/A_{\text{G}} = 8.2$  for  $\text{SWCNT}(\text{COOH})_n$  (THF/ultrasound) (3). Furthermore, for this respective  $\text{SWCNT}$  derivative, the intensity increase of the D-band is much less pronounced ( $A_{\text{D}}/A_{\text{G}} = 3.0$ ) when an excitation wavelength of 532 nm is chosen, where predominantly metallic tubes are in resonance.<sup>52</sup> An intermediate situation is observed for the excitation at 633 nm, where both metallic and semiconducting  $\text{SWCNT}$  species can be probed. In this case, the ratio of  $A_{\text{D}}/A_{\text{G}}$  is 5.1. These results are a clear indication for a preferred functionalization of semiconducting  $\text{SWCNTs}$ . Such a behavior is unprecedented<sup>30,31,33–35</sup> for any established reductive functionalization sequence.

An even more detailed insight into this unexpected selectivity is provided by the analysis of the radial breathing mode (RBM) region of the respective Raman spectra. The close investigation of the RBM region (Figure 2) further supports the finding of a preferred covalent functionalization of semiconducting  $\text{SWCNTs}$ , which is indicated by a significant relative intensity increase of the RBM bands of metallic tubes as compared to almost vanishing semiconducting RBM signals.

Such characteristic functionalization-induced changes of the RBM intensities will be discussed in detail below with the example of  $\text{SWCNT}(\text{COOH})_n$  (THF/ultrasound) (3). At 532 nm excitation (Figure 2b), mainly metallic tubes (gray colored ( $n,m$ )-indices), except for two large and small diameter semiconducting tubes (black colored ( $n,m$ )-indices), (14,4), (14,1) and (9,2), (10,0), are detected in the RBM region.<sup>53</sup> After functionalization, the intensities of the signals of metallic  $\text{SWCNT}$  chiralities are significantly increased as compared to those of the semiconducting species, which is again a clear indication for the preferred functionalization of the latter. Moreover, the signal of the larger diameter metallic tubes, (9,6), (10,4), (11,2), and (7,7), is apparently increasing as compared to the corresponding smaller diameter species, (8,5) and (9,3). The underlying preferred attack of the intermediately generated radical onto tubes with smaller diameter is in line with the preferred functionalization of smaller diameter semiconducting tubes. Here, only the bands of larger diameter species, (14,4) and (14,1), can barely be detected, whereas the resonance signals of the smaller diameter tubes (9,2), (10,0) have completely vanished.

These conclusions are corroborated by the spectra obtained with an excitation wavelength of 633 nm (Figure 2c). Here, the RBMs of the metallic tube signals appear in the low frequency region ( $180\text{--}250\text{ cm}^{-1}$ , gray colored ( $n,m$ )-indices) of the spectrum, whereas the signals of the semiconducting tubes are located in the high frequency region ( $250\text{--}300\text{ cm}^{-1}$ , black colored ( $n,m$ )-indices). After functionalization, the signals of all metallic  $\text{SWCNTs}$  are significantly increased as compared to those of the as-received starting material ( $p$ - $\text{SWCNTs}$ ). Again, a dramatic intensity decrease for the semiconducting carbon nanotube species is detected, which becomes even more evident in the spectrum recorded at 785 nm excitation (Figure 2d). Besides the large diameter tubes ((13,3) and (14,1)), only the signals of the (10,2) and (11,0) chiralities, which exhibit a pronounced intensity in the starting material, can barely be observed. All other signals for semiconducting tubes have completely disappeared.

It has been outlined previously that an analytical interpretation of the Raman spectra based on only three excitation energies has to be taken with care, because additional to the covalent addend binding also the sample morphology may have an influence on the intensities of the Raman RBM signals.<sup>48</sup> In general, the covalent functionalization of carbon nanotubes leads to a red-shift of the resonance window, resulting in an intensity decrease of the RBMs.<sup>48</sup> However, due to a pronounced debundling of sidewall carboxylated  $\text{SWCNT}(\text{COOH})_n$ , the resonance window is narrowed, and the  $\text{SWCNT}$  transition energies are up-shifted due to a weaker intertube coupling. This leads to an increase or decrease of the corresponding RBM intensity depending on the localization of the  $\text{SWCNT}$  species in the resonance window.<sup>54–56</sup> Accordingly, functionalization and the derivatization-induced debundling result in two contrary effects, red-shift and blue-shift of the resonance window, respectively. Therefore, an accurate assignment and discussion of the RBM region cannot solely be based on three distinct excitation wavelengths. Hence, to exclude the possibility that the spectral changes discussed above are induced by a shift of the resonance window, we carried out an in-depth Raman characterization of  $\text{SWCNT}(\text{COOH})_n$  (THF/ultrasound) (3), where the laser excitation energy has been tuned between 564 and 613 nm. The corresponding RBM plots are depicted in Figure S5, and two fundamental conclusions can be drawn from the data obtained: (a) the reductive carboxylation is a diameter selective addition reaction, preference of small diameter tubes, no matter what reaction conditions are chosen for the derivatization; and (b) under ultrasonic agitation of the reduced  $\text{SWCNT}^{n-}$  intermediates, an electronic type selective reaction takes place, where semiconducting  $\text{SWCNT}$  species are preferably functionalized, whereas their metallic counterparts remain unfunctionalized except for the very reactive small diameter chiralities. In the case of the high pressure functionalization sequences, the increasing degrees of functionalization of the bulk materials are accompanied by a progressive functionalization of medium and large diameter metallic species.

**Discussion of the Underlying Selectivity.** The preferred covalent functionalization of semiconducting  $\text{SWCNTs}$  clearly demonstrated within this article is a puzzling issue, as it has thus far not been observed. If at all, selectivity toward metallic  $\text{SWCNT}$  species has been reported up to now.<sup>30,31,33–35</sup>

To gain further insights, we have extended our investigations to standard Billups chemistry, the reaction of the reduced  $\text{SWCNT}^{n-}$  intermediates with alkyl halogenides (Scheme S1). Herein, the reaction of perfluorobutyl iodide (PFBi) with  $\text{SWCNTs}$  under modified conditions, without ultrasonic treatment (Scheme S1a), yields a sidewall derivatized material  $\text{SWCNT}(\text{PFBi})_n$  (THF) (7) with an  $A_{\text{D}}/A_{\text{G}}$  ratio of 7.7 (633 nm, Figure S6b), indicative of an effective sidewall addition of the intermediately generated alkyl radicals. However, no electronic type specific  $\text{SWCNT}$  functionalization can be derived from the respective Raman data presented in the Supporting Information (Figures S6, S7). This picture totally changes with ultrasonic agitation of the reaction mixture containing the reduced  $\text{SWCNT}^{n-}$  species prior to the addition of the perfluorobutyl iodide. First, the Raman determined degree of functionalization for  $\text{SWCNT}(\text{PFBi})_n$  (THF/ultrasound) (8) is dramatically increased by a factor of approximately 3 ( $A_{\text{D}}/A_{\text{G}} = 22.4$ ) as compared to the procedure without ultrasonic treatment. The corresponding  $A_{\text{D}}/A_{\text{G}}$  values for the excitation wavelengths 532 and 785 nm are supplied in Figure S6a and S6c. Second, as is clearly discernible by a close inspection of the RBM regions

(Figures S7), the Raman bands for the semiconducting species have vanished almost completely, whereas the signals for the metallic SWCNTs can still be detected, indicative of a highly preferred reaction of the semiconducting tubes. Again, this analysis is fully consistent with the experimental data obtained from the respective Raman RBM screening of the functionalized material SWCNT(PFBI)<sub>n</sub> (THF/ultrasound) (8) with tunable excitation energies between 565 and 629 nm (see Figure S8).

Accordingly, the electronic-type selectivity appears to be independent of the electrophile used during the addition reaction. Furthermore, the ultrasonic treatment of the SWCNT<sup>n-</sup> intermediates seems to be a fundamental key element. We rationalize our observation in terms of a preferential reactivity of doped semiconducting SWCNTs, similar to the explanation given by Miyata et al. who observed an electronic type specific oxidation where semiconducting SWCNTs were oxidized by hydrogen peroxide preferentially over their metallic counterparts.<sup>57</sup> They explained this observation in terms of a hole-doping mechanism of the SWCNTs. Later, this explanation was confirmed by a computational study of Lu et al.<sup>58</sup> revealing that the selective adsorption of H<sub>2</sub>O<sub>2</sub> on semiconducting SWCNTs is accompanied by p-type doping, which results in a shift of the Fermi level toward the first van Hove singularity (vHS) of the semiconducting SWCNT's valence band.<sup>57</sup> This causes a drastic increase of allowed states in the proximity of the Fermi level, even compared to the metallic tubes, stabilizing the intermediate state of the reaction and therefore resulting in a preferential derivatization of semiconducting species.

This explanation is perfectly in line with the selectivity toward metallic nanotubes in the case of undoped SWCNTs, especially because it is well-known from solid-state physics that the Fermi level in semiconductors is much more sensitive toward doping effects than that of metallic species. In the case of the metallic species, the Fermi energy is equivalent to the work function, which is almost independent of the injection of charge to the metal. In contrast, even a slight doping of a semiconductor introduces donor or acceptor states close to the edges of the band gap, and for higher doping levels the semiconductor degenerates, shifting the Fermi energy into either the valence or the conduction band. Upon transferring this knowledge to the scenario of carbon nanotube chemistry, it becomes evident that the reactivity of charged metallic SWCNTs is not dramatically different from the behavior of the uncharged pristine material as the density of states (DOS) remains constant during doping. This is in marked contrast to semiconducting SWCNTs where charging during the reaction (or doping) induces a dramatic shift of the Fermi level, resulting in a higher reactivity of these SWCNT species relative to their metallic counterparts. This is in excellent agreement with the observed data and the report from Paolucci et al.<sup>59</sup>

Whenever the Fermi level approaches the first van Hove singularity, this SWCNT chirality will become preferentially functionalized. From this point of view, the selectivity is based on the Fermi level of the nanotubes after reduction and would be independent of the chemical identity of the functional group itself. However, because the selective functionalization of semiconducting SWCNTs has not been experimentally observed up to the current contribution, another piece in the jigsaw puzzle is obviously missing, which we believe can be found in the ultrasonic treatment as a key element.

As outlined above, the ultrasonic agitation of the THF solution with the reduced SWCNT<sup>n-</sup> species is a fundamental prerequisite for the selectivity of the subsequent addition reaction by CO<sub>2</sub>

or perfluorobutyl iodide. This ultrasonication step boosts the Coulomb-based debundling of aggregated SWCNTs, yielding exfoliated species that can be individually addressed by the electrophilic trapping reagent. In the case of insufficiently debundled samples, such an electronic type selective discrimination does not take place, as has been previously reported by our group and by the group of Penicaud.<sup>33,60</sup> In the reduced bundled material, a homogenization of the charge density due to electronic communication among all SWCNT chiralities yields a common average Fermi level, and therefore no selectivity toward a distinct electronic type can be observed. Moreover, the notable increase in the degree of functionalization between the nonultrasonically treated SWCNT<sup>n-</sup> solution, for instance, SWCNT(PFBI)<sub>n</sub> (THF) (7) ( $A_D/A_G$  (633 nm) = 7.7), and the sample with ultrasonic agitation, SWCNT(PFBI)<sub>n</sub> (THF/ultrasound) (8) ( $A_D/A_G$  (633 nm) = 22.4), can be explained by the increase of accessible surface area upon SWCNT debundling. As described above, the reactivity of charged metallic SWCNTs is not dramatically different from the uncharged pristine material as the DOS remains constant during doping. This is in marked contrast to the semiconducting SWCNTs, where charging (or doping) during the reaction induces a dramatic shift of the Fermi level, resulting in a higher reactivity of these SWCNT species relative to the metallic counterparts. In the present reduction, the Fermi level is supposed to match the first semiconducting vHS, whereas the metallic ones remain unaffected.

Additional aspects such as the redox potential of the electrophile with respect to the Fermi level of the charged SWCNT intermediates will also have an impact on the experimentally observed selective derivatization of semiconducting SWCNTs. Further efforts to fully elucidate the underlying mechanism are currently underway in our research group.

**Absorption Spectroscopy and Solubility.** As was already demonstrated above, the reductive carboxylation of SWCNT under ultrasonic treatment is a highly versatile reaction with respect to diameter and electronic type selectivity, but also with respect to the fine-tuning of the degree of functionalization by external stimuli such as pressure. This opens the door for an extensive investigation of the spectroscopic properties of SWCNT derivatives with the same functional entity, but with varying degrees of functionalization. To gain insights into the optical characteristics and the dispersibility of the sidewall carboxylated SWCNT derivatives in comparison to their as-received counterparts, two samples with medium (SWCNT(COOH)<sub>n</sub> (THF/ultrasound) (4)) and high (SWCNT(COOH)<sub>n</sub> (THF/ultrasound/55 bar) (6)) degrees of functionalization ((4)  $A_D/A_G$  (633 nm) = 9.3, (6)  $A_D/A_G$  (633 nm) = 21.7) were investigated by UV-vis-nIR absorption spectroscopy.

Because it has been shown that N-methyl-2-pyrrolidone (NMP) is a highly suitable solvent for the dispersion of SWCNTs,<sup>61–64</sup> the sidewall carboxylated nanotubes were dispersed in dry NMP by the aid of bath type sonication, and the homogeneous dispersions were then centrifuged to remove coarse aggregates and insoluble material. The corresponding absorption spectra of the respective supernatant solutions, normalized to the local minimum at 920 nm, are displayed in Figure 3a. Furthermore, the absorbance intensity at 660 nm as well as the respective SWCNT concentrations are summarized in Table 2.

At first glance, it may appear surprising that the highly functionalized SWCNTs (6) are less efficiently dispersed in NMP as compared to the medium functionalized derivatives (4) or the pristine starting material, as it is commonly believed

that nanotube solubility is increased by the covalent attachment of functional entities. However, as was recently shown by Coleman and co-workers, this will be only the case if the Hildebrand parameter of the functional entity matches that of the solvent.<sup>65</sup> Accordingly, it is quite reasonable that the solubility of the nanotubes with high degrees of functionalization is governed by the functional moieties and no longer by the nanotube itself, inducing a decreased dispersion efficiency in SWCNT solvents such as NMP. The absorption spectra displayed in Figure 3 reveal dramatic changes in the intensity and relative distribution of the characteristic SWCNT excitonic transitions directly related to the van Hove singularities in the electronic density of states of the 1D carbon allotrope.<sup>66,67</sup> This can be traced back to the broadening and to a red-shifting of the optical transitions by the introduction of the  $sp^3$ -defects upon sidewall functionalization,<sup>68–71</sup> which eventually leads to a complete loss of the characteristic signals. In the case of the medium functionalized SWCNT derivative SWCNT-(COOH)<sub>n</sub> (THF/ultrasound) (4), the transitions related to metallic SWCNTs ( $M_{11}$ ), as well as those stemming from larger diameter semiconducting SWCNTs ( $S_{11}$  and  $S_{22}$ ), are still reasonably well resolved. This strongly supports the preferred carboxylation of small diameter semiconducting nanotubes. The highly carboxylated material in turn is characterized by the nearly complete loss of all SWCNT transitions.

To demonstrate that SWCNT dispersibility can indeed be strongly increased by the covalent sidewall modification, we have turned to THF as a solvent, where pristine SWCNTs are virtually insoluble. To avoid unwanted aggregation of the material upon drying, samples were immediately dispersed in THF by sonication after the wet chemical processing and the functionalization. The dispersions were again mildly centrifuged (5 krpm, 10 min) to remove the coarse aggregates and subjected to absorption spectroscopy. The initial SWCNT concentrations and the

supernatant concentrations were determined gravimetrically after removal of the solvent. Significantly, the dispersion efficiency in THF could be increased from approximately 0 to 87% by the covalent attachment of the carboxylic acid functionalities, indicating that THF is a highly potent solvent for carboxylated SWCNTs in contrast to the nonfunctionalized counterparts (Table 3). A respective absorption spectrum is depicted in Figure 3b.

Because the absorption plots of the functionalized material in general are characterized by an almost complete absence of the characteristic SWCNT transitions (especially in the THF dispersion), the question arises whether this is traced back to a lack of debundling or to the covalent modification of the nanotube network. To clarify this issue, the morphology of the spin-casted THF dispersions was investigated by atomic force microscopy.

**Table 2. Absorbance Intensity at 660 nm of the Supernatant Dispersions of Pristine HiPCO SWCNTs (P0261) in Comparison to Carboxylated SWCNTs with Medium (SWCNT-(COOH)<sub>n</sub> (THF/Ultrasound) (4)) and High (SWCNT(CO OH)<sub>n</sub> (THF/Ultrasound/55 bar) (6)) Degrees of Functionalization in NMP<sup>a</sup>**

	p-SWCNT	4	6
absorbance Intensity	1.72	1.76	1.12
$c_s$ (SWCNT)/g L <sup>-1</sup>	0.053 ± 0.003	0.054 ± 0.0045	0.034 ± 0.005
dispersibility in NMP	53% ± 3%	54% ± 4.5%	34% ± 5%

<sup>a</sup> The nanotube concentrations in the supernatant ( $c_s$ ) can be calculated from the extinction coefficient of HiPCO SWCNTs in NMP.<sup>65</sup> The dispersibility is directly deduced from the ratio of the initial SWCNT concentrations 0.1 g L<sup>-1</sup> to the actual concentrations in the supernatant. The (3-fold) repetition of the experiment yields an experimental error of maximum ±5%.

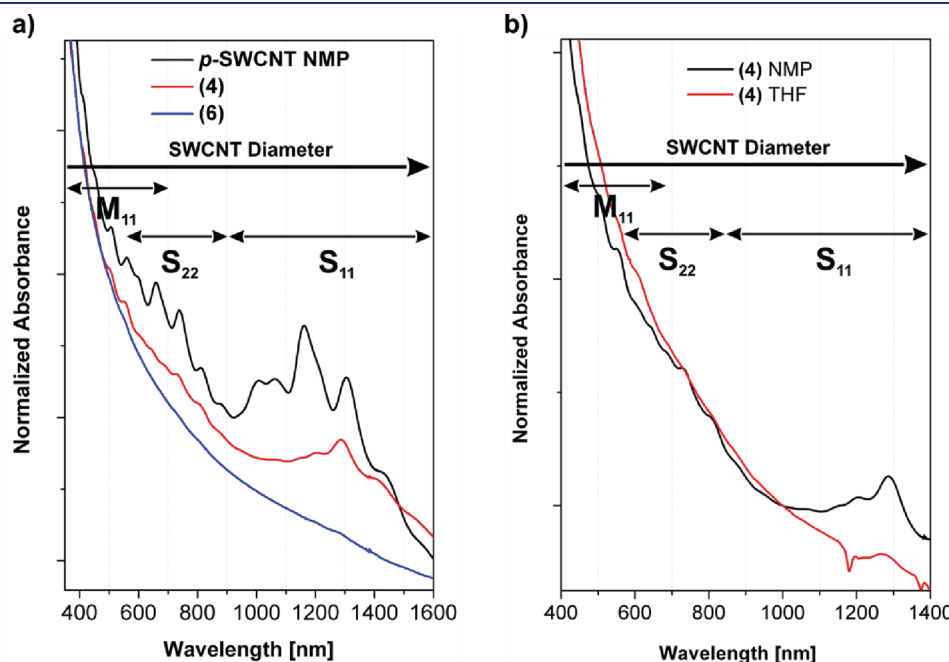


**Figure 3.** (a) UV-vis/nIR absorption spectra of as-received *p*-SWNTs, SWCNT(COOH)<sub>n</sub> (THF/ultrasound) (4), and SWCNT(COOH)<sub>n</sub> (THF/ultrasound/55 bar) (6) in NMP normalized to the local minimum between semiconducting  $S_{22}$  and  $S_{11}$  transitions at 920 nm; spectra offset for clarity. In all cases, the supernatant after centrifugation (20 min, 15 krpm) is displayed. (b) UV-vis/nIR absorption spectra of medium functionalized HiPCO SWCNTs (SWCNT(COOH)<sub>n</sub> (THF/ultrasound) (4)) in NMP and THF normalized to the local minimum between semiconducting  $S_{22}$  and  $S_{11}$  transitions at 920 nm.

**Table 3.** Dispersion Efficiencies in THF (Gravimetrically Determined) of Pristine SWCNTs and Carboxylated SWCNTs with Medium (SWCNT(COOH)<sub>n</sub> (THF/Ultrasound) (4)) and High (SWCNT(COOH)<sub>n</sub> (THF/Ultrasound/55 bar) (6)) Functionalization Degrees, Respectively

	p-SWCNT	4	6
dispersibility in THF	<1%	15% ± 5%	84% ± 4.5%

As revealed by the representative images in Figure S9, the nanotubes are well dispersed and individualized so that the loss of the transitions in the absorption spectra is predominantly attributed to the covalent derivatization.

**Emission Spectroscopy.** SWCNT photoluminescence has evolved to a powerful characterization tool, as the excitonic transitions of individualized semiconducting SWCNTs, which are directly related to the density of states and therefore to the SWCNT chirality, can be probed.<sup>72</sup> Thus, the sample composition (of semiconducting SWCNTs) can be conveniently mapped from the excitation–emission characteristics.<sup>73,74</sup> For this purpose, the two sidewall carboxylated SWCNT samples, SWCNT-(COOH)<sub>n</sub> (THF/ultrasound) (4) and SWCNT(COOH)<sub>n</sub> (THF/ultrasound/55 bar) (6), were dispersed in a 2 wt % aqueous solution of sodium deoxycholic acid (SDC, [SWCNT]<sub>i</sub> = 0.1 g L<sup>-1</sup>) by bath type sonication (20 min) and centrifuged (20 min at 15 krpm). The supernatant was then diluted to an absorbance intensity of 0.04 per 1 cm path length at 660 nm, and the nIR emission was recorded at an excitation of 660 nm. We have turned to aqueous surfactant solutions instead of the solubilization in organic media such as NMP where the SWCNTs can be stably dispersed without additives, as it has been shown that the nIR emission is commonly reduced by a factor of 50–100 in NMP dispersions in comparison to aqueous surfactant solutions of similar optical densities and individualization rates.<sup>63</sup>

As the introduction of sp<sup>3</sup>-carbon atoms into the nanotube scaffold induces changes in the electronic structure of the SWCNTs, nanotube emission intensities of functionalized SWCNTs are commonly drastically reduced.<sup>68,75,76</sup> The emission intensity of SWCNT(COOH)<sub>n</sub> (THF/ultrasound) (4) in SDC is reduced by a factor of 45 (Figure 4) as compared to the pristine SWCNTs at the same optical density. Significantly, the nIR fluorescence in the case of SWCNT(COOH)<sub>n</sub> (THF/ultrasound/55 bar) (6) has totally vanished, pointing toward a complete functionalization of all semiconducting SWCNTs.

The diameter selectivity that accompanies the preferential carboxylation of semiconducting SWCNT species can easily be evidenced by a direct comparison of the emission spectra of SWCNT(COOH)<sub>n</sub> (THF/ultrasound) (4) and of the as-received starting material. The relative intensities of the residual emission attributed to specific (n,m)-SWCNTs undergo intense redistributions in the functionalized sample. This is most striking for the higher energy region of the spectrum at wavelengths below 1100 nm, as no nIR emission is detected. This region can be attributed to SWCNT species with diameters smaller than 0.9 nm,<sup>73</sup> which constitute the most reactive species for this derivatization sequence. Accordingly, they are heavily functionalized, resulting in a complete loss of their emission.

**The Chemical Identity of the Functional Group.** To prove the chemical identity of the functional moieties grafted onto the SWCNT sidewall, the sample with the highest functionalization degree SWCNT(COOH)<sub>n</sub> (THF/ultrasound/55 bar) (6) has

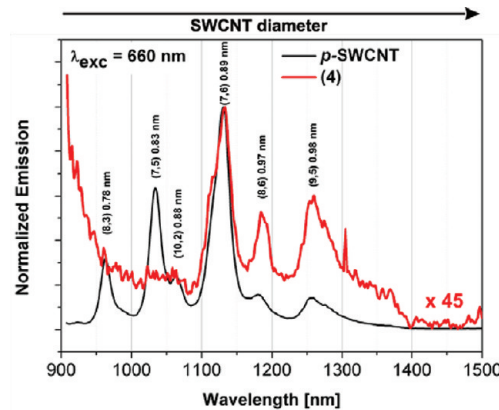


**Figure 4.** nIR emission spectra of carboxylated SWCNTs with medium functionalization degrees, SWCNT(COOH)<sub>n</sub> (THF/ultrasound) (4), as compared to the pristine material normalized to the local maximum at 1130 nm. In both cases, the SWCNTs were dispersed in a 2 wt % aqueous solution of SDC, centrifuged, and diluted to an absorbance intensity of 0.04 at the excitation wavelength of 660 nm.

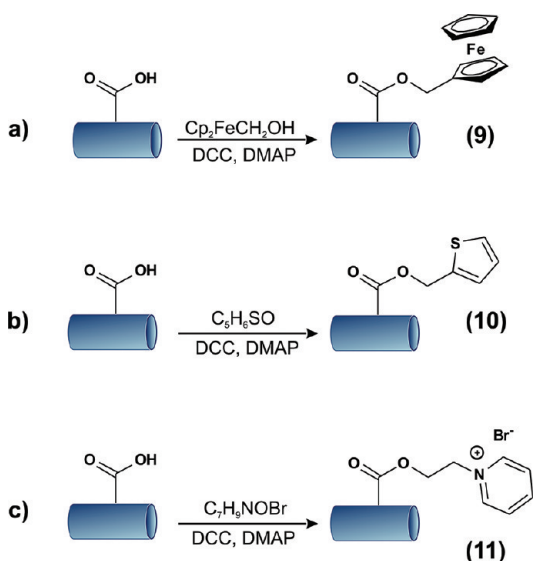
been subjected to IR spectroscopy. On the basis of the spectral data (Figure S10), carboxylic acid functionalities have been attached on the SWCNT scaffold, as the C=O stretching mode at 1715 cm<sup>-1</sup> is observed together with the O–H deformation mode (O–H δ) at 1440 cm<sup>-1</sup>.

Further support for the presence of carboxylic acid functionalities can be derived from zeta potential measurements (detailed information, see Supporting Information). In the case of neutral colloidal particles, the zeta potential changes from positive to negative values upon increasing the pH. Commonly, a pH titration results in a sigmoidal curve with an inflection point that is equal to the isoelectric point where the zeta potential is zero. Herein, the zeta potential values of the pH titration of the highly functionalized SWCNT(COOH)<sub>n</sub> (THF/ultrasound/55 bar) (6) in the range of pH = 2 to pH = 7 (Figure S11) can actually be fitted to a sigmoidal curve. The inflection point of the titration curve is determined to be at pH = 4.7 with a zeta potential of -15.5 mV. This unambiguously proves the presence of pH active moieties, as the inflection point is not equal to the isoelectric point. Additionally, a pH value of 4.7 at the inflection point, being identical to the respective pK<sub>a</sub> value, strongly suggests that these pH-active moieties are carboxylic acid functionalities.

This implication is furthermore substantiated by the corresponding data obtained by a mass spectrometric coupled thermogravimetric analysis (TGA-MS) of the carboxylated material. In Figure S12 (Supporting Information), the respective mass loss profile in combination with the detected ion current for CO<sub>2</sub> (*m/z* = 44) of SWCNT(COOH)<sub>n</sub> (THF/ultrasound) (3) are depicted. Herein, the desorption of CO<sub>2</sub> can be monitored over the complete temperature regime, ranging from 100 to 700 °C. Nevertheless, the maximum of the ion current is allocated between 300 and 400 °C, which corresponds to the temperature region where covalent C–C bonds are cleaved. On the basis of the detected mass loss in this temperature regime (~4.5%), the respective average degree of functionalization for the bulk material can be calculated, yielding functionalization degrees of 3.1%, which corresponds to a derivatization of every 33rd carbon atom of the nanotube framework.

As outlined above, the reductive sidewall polycarboxylation by the use of gaseous carbon dioxide yields functional SWCNT

**Scheme 2. DCC-Mediated Coupling of Functional Alcohols with Sidewall Carboxylated SWCNTs Yielding the Corresponding Functional Adducts: (a) SWCNT(COO-ferrocenylmethyl)<sub>n</sub> (9), (b) SWCNT(COO-thiophenylmethyl)<sub>n</sub> (10), and (c) SWCNT(COO-ethylpyridinium bromide)<sub>n</sub> (11)**



derivatives with covalently bound carboxylic acid functionalities, a versatile anchoring unit for subsequent derivatization procedures. On the basis of that, the extensive portfolio of defect functionalization sequences<sup>21,77</sup> can now, for the first time, be transferred to structurally integer carbon nanotubes. We used this potential of subsequent functional entity coupling for the proof of the chemical identity of the carboxylic acid functionalities introduced by our novel reaction sequence. Ferrocenemethanol, 2-thiophenemethanol, and *N*-(hydroxyethyl)pyridinium bromide<sup>78</sup> were linked to the carboxylic anchors of functionalized nanotubes (3) applying standard DCC activated ester coupling conditions (Scheme 2), and the respective SWCNT derivatives have been investigated in detail by mass-spectrometric coupled TGA.

For the ferrocenemethanol coupled SWCNT derivative SWCNT(COO-ferrocenylmethyl)<sub>n</sub> (9), the respective TGA trace in combination with the ion currents of the detected cyclopentadienyl fragments is depicted in Figure S13 (Supporting Information). Herein, the major mass loss occurs in the temperature range between 300 and 550 °C (20.8% mass loss) and is accompanied by the detection of the two characteristic cyclopentadienyl fragments, *m/z* = 65 ( $C_5H_5$ ) and *m/z* = 94 ( $C_5H_4-CH_2OH$ ), of the covalently coupled ferrocenemethyl unit. The mass loss allocated in the temperature region between 100 and 300 °C can be attributed to remaining traces of adsorbed ferrocenemethanol.

In a reference experiment, ferrocenecarboxylic acid was used under the same coupling conditions as were applied in the case of ferrocenemethanol (Scheme 2a). In the resulting SWCNT sample, no characteristic signal for the cyclopentadienyl ring can be detected by TGA-MS (Figure S14, Supporting Information). This demonstrates the feasibility of the postcoupling analysis of carboxylated SWCNTs by mass-spectrometric coupled TGA and can be taken as proof of the chemical identity for the covalent grafting of carboxylic acid functionalities onto the SWCNT sidewalls.

To demonstrate the versatility of the sidewall bound carboxylic acid functionalities for subsequent derivatization reactions, 2-thiophenemethanol and *N*-(hydroxyethyl)pyridinium bromide, respectively, were also coupled under Steglich conditions, and the corresponding fragments of the addends could be detected by TGA-MS for SWCNT(COO-thiophenylmethyl)<sub>n</sub> (10) (Figure S15, Supporting Information) and SWCNT(COO-ethylpyridinium bromide)<sub>n</sub> (11) (Figure S16, Supporting Information), respectively.

**Separation of the Sidewall Carboxylated SWCNTs by Density Gradient Ultracentrifugation.** Despite the fact that semiconducting SWCNTs exhibit a more pronounced reactivity under carefully explored reaction conditions with tunable degrees of functionalization, a major obstacle is still presented in the clear and efficient separation of the functionalized from the nonfunctionalized material. This not only hinges on the potential future applicability of this derivatization sequence with regard to scalable SWCNT sorting, but furthermore strongly complicates the characterization of the SWCNT bulk material. A powerful methodology to overcome this problem is presented in density gradient ultracentrifugation (DGU), as it has been shown that covalently derivatized SWCNTs exhibit significantly higher buoyant densities in aqueous surfactant solutions as compared to their nonfunctionalized counterparts.<sup>79</sup> Furthermore, we have recently applied this technique for the separation of defectous SWCNTs from structurally integer material.<sup>80</sup> To demonstrate the versatility of the DGU approach for the sorting of the reductively carboxylated SWCNTs and the benefits arising from this separation with regard to the precise characterization of the nanotubes, two samples with different degrees of carboxylation (SWCNT(COOH)<sub>n</sub> (THF/ultrasound) (4) and SWCNT(COOH)<sub>n</sub> (THF/ultrasound/55 bar) (6)) have been subjected to DGU. In our case, the protocol established by Strano<sup>79</sup> has been slightly modified to separate the nonfunctionalized from the functionalized and the bundled material in a single DGU step. The setup is summarized in Figure S17 (Supporting Information) and in the Experimental Section. After 17.5 h of centrifugation at 40 krpm, three spatially separated bands are observed and fractionated (denoted as F1, F2, F3 from top to bottom). The topmost fraction F1 contains individualized nonfunctionalized SWCNTs, the second fraction F2 the functionalized (or defectous) counterparts, and fraction F3 the bundled SWCNTs (Figure S17, Supporting Information).

To (a) proof the successful sorting of nonfunctionalized and functionalized SWCNTs, (b) illustrate the selectivity of the covalent functionalization sequence, and (c) provide a detailed characterization of the carboxylated SWCNTs, the fractions F1–F3 of both DGU experiments with as-received SWCNTs, medium functionalized (SWCNT(COOH)<sub>n</sub> (THF/ultrasound) (4)), and highly functionalized SWCNTs (SWCNT(COOH)<sub>n</sub> (THF/ultrasound/55 bar) (6)) have been subjected to extensive measurements by absorption, emission, and Raman spectroscopy and AFM as outlined and discussed in detail in the Supporting Information (Figures S18, S19) and compared to *p*-SWCNTs processed under equal conditions. Because fraction F2 always contains an unknown contribution of defectous nanotubes, which are also present in the as-received HiPCO SWCNTs, a detailed comparison of the F2 of different SWCNT samples needs to be, if at all, carried out with care, except for an evaluation of the Raman  $A_D/A_G$  ratios (Figure 5). The respective Raman spectra are displayed in Figure S20 (Supporting Information). It should be noted that the values plotted in Figure 5 are the ratios

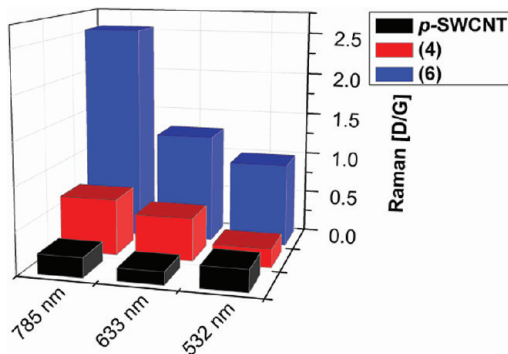


**Figure 5.** Direct comparison of the Raman  $A_D/A_G$  ratios of fractions F2 collected from as-received SWCNTs, SWCNT(COOH)<sub>n</sub> (THF/ultrasound) (4), and SWCNT(COOH)<sub>n</sub> (THF/ultrasound/55 bar) (6) recorded from the solid at three excitation wavelengths, 532, 633, and 785 nm.

of the D-band integral and the G-band integral (without reference to the pristine material). The comparison is nonetheless appealing, as the actual  $A_D/A_G$  ratios of the material without contributions from amorphous carbon or varying bundling degrees can be deduced after the DGU sorting.

Even though fraction F2 is always characterized by a higher defect density than fraction F1 (Figures S18 and S19), the differences between the as-received pristine nanotubes as compared to the functionalized material are striking. In case of medium functionalized SWCNT(COOH)<sub>n</sub> (THF, ultrasound) (4), the  $A_D/A_G$  ratio at 532 nm excitation where predominantly metallic SWCNTs are in resonance even falls below the value for the pristine material, further evidencing the preferential derivatization of the corresponding semiconducting nanotubes. These species are predominantly excited at 785 nm, giving rise to an enhanced  $A_D/A_G$  ratio with respect to the as-received starting material. Furthermore, the nanotubes functionalized at elevated pressure (SWCNT(COOH)<sub>n</sub> (THF/ultrasound/55 bar) (6)) are characterized by a drastically higher defect density (and therefore functionalization degree) at all excitation wavelengths, as (small diameter) metallic SWCNT species are also successfully carboxylated. The  $A_D/A_G$  ratio at 785 nm excitation is in this system nonetheless significantly higher than for the other two excitation energies. These results are perfectly in line with the data obtained from the bulk material and emphasize the potential of the reductive polycarboxylation sequence with respect to selectivity and tuning of the functionalization degree by external stimuli such as pressure.

Furthermore, the pronounced selectivity toward a preferred derivatization of semiconducting SWCNT chiralities is also nicely reflected in the absorption spectra of the nonfunctionalized cross sections (F1) of SWCNTs of the as-received nanotubes as compared to the SWCNT(COOH)<sub>n</sub> (THF/ultrasound) (4) and SWCNT(COOH)<sub>n</sub> (THF/ultrasound/55 bar) (6) samples (Figure 6a). Herein, the fractions F1 after DGU sorting exhibit an enhanced enrichment of metallic (or rather depletion of semiconducting) SWCNT species with increasing bulk functionalization degrees.

This trend is further corroborated by the nIR fluorescence spectral intensities (Figure 6b and Table 4), which drop dramatically in the functionalized samples at equal absorbance intensities (0.04 at 660 nm) and accordingly similar SWCNT concentrations. In the case of the SWCNT(COOH)<sub>n</sub> (THF/ultrasound/55 bar)

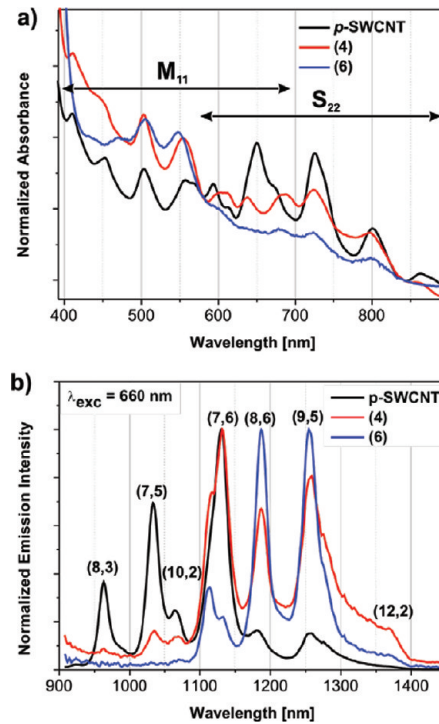


**Figure 6.** (a) Optical absorption spectra normalized to 830 nm of fractions F1 after DGU sorting of as-received HiPCO SWCNTs (F1) as compared to HiPCO SWCNT samples that have been moderately, SWCNT(COOH)<sub>n</sub> (THF/ultrasound) (4), and highly, SWCNT(COOH)<sub>n</sub> (THF/ultrasound/55 bar) (6), functionalized. (b) Emission spectra with an excitation wavelength of 660 nm normalized to the respective maximum of fractions F1 after DGU sorting of p-SWCNTs, and (4) and (6) SWCNT samples. The SWCNT (*n,m*) indices of the respective peaks are indicated.

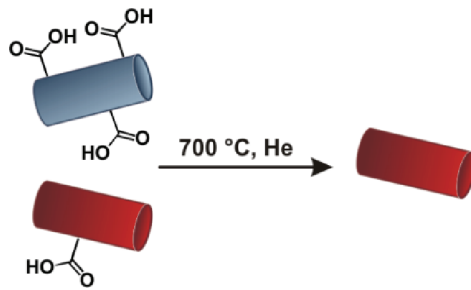
(6), the nIR emission intensity of, for example, the (7,6)-SWCNT ( $d = 0.89$  nm) is reduced to 0.2% of the intensity of the respective tube in F1 of the as-received starting material. Therefore, we conclude that no semiconducting SWCNTs remain unfunctionalized with diameters smaller than 0.9 nm. The abundance of the (8,6)-SWCNT with a diameter of 0.97 nm is also drastically reduced to 5.2%. Accordingly, an enrichment factor of metallic SWCNTs in the nonfunctionalized fraction F1 after DGU of SWCNT(COOH)<sub>n</sub> (THF/ultrasound/55 bar) (6) can be estimated to be greater than 95% and even 92.5% for the medium functionalized sample SWCNT(COOH)<sub>n</sub> (THF/ultrasound) (4). Please note that this comparison is only valid because SWCNTs in DGU fractions F1 are individualized and defect free.

The underlying preferred functionalization of smaller diameter SWCNTs can best be followed in the normalized emission spectra (with an excitation wavelength of 660 nm), with an intense redistribution of the peaks attributed to the excitonic transitions of different (*n,m*)-SWCNTs occurs (Figure 6b). Please note that the spectra are much better resolved in comparison to the spectral features presented in Figure 4, especially in the case of the highly functionalized samples, where no nIR emission was detected in the bulk sample prior to DGU, due to the low concentration of individualized nonfunctionalized semiconducting SWCNTs. In SWCNT(COOH)<sub>n</sub> (THF/ultrasound) (4), the peaks attributed to the nanotubes with diameters smaller than 0.8 nm (for example, the (8,3) and (7,5) SWCNTs) almost vanish, as they are obviously completely functionalized,

**Table 4.** Tabulated Emission Intensities of Chosen SWCNT Chiralities in the Nonfunctionalized Fraction F1 after DGU Sorting of As-Received *p*-SWCNT, SWCNT(COOH)<sub>n</sub> (THF/Ultrasound) (4), and SWCNT(COOH)<sub>n</sub> (THF/Ultrasound/55 bar) (6) and the Deduced Relative Abundance of the (n,m) SWCNTs with Respect to the As-Received Starting Material

sample	emission position/nm	(n,m)	SWCNT diameter/nm	emission intensity/nW cm <sup>-1</sup>	relative abundance
<i>p</i> -SWCNT	1033	(7,5)	0.83	$2.7 \times 10^{-9}$	100%
	1131	(7,6)	0.89	$3.9 \times 10^{-9}$	100%
	1186	(8,6)	0.97	$6.3 \times 10^{-10}$	100%
4	1033	(7,5)	0.83	$1.1 \times 10^{-11}$	0.4%
	1131	(7,6)	0.89	$6.9 \times 10^{-11}$	1.8%
	1186	(8,6)	0.97	$4.7 \times 10^{-11}$	7.5%
6	1033	(7,5)	0.83	0	0%
	1131	(7,6)	0.89	$7.2 \times 10^{-12}$	0.2%
	1186	(8,6)	0.97	$3.3 \times 10^{-11}$	5.2%

**Scheme 3.** Schematic Representation of the High Temperature Constructive Destruction of the Highly Functionalized Semiconducting SWCNT Material (Blue) in Combination with the Thermal Defunctionalization of the Little Functionalized Metallic Systems (Red)



whereas in SWCNT(COOH)<sub>n</sub> (THF/ultrasound/55 bar) (6) traces of unfunctionalized semiconducting SWCNTs can be attributed to SWCNTs with diameters larger than 0.9 nm (for example, the (8,6) and (9,5) tubes).

**Selective Constructive Destruction by Thermal Annealing.** The pristine form of covalently functionalized SWCNTs can be thermally recovered by heating the sample under inert gas atmosphere. Hereby, most of the sp<sup>3</sup> carbon atoms are transformed back to sp<sup>2</sup> carbon species by this defunctionalization routine.<sup>70,81–84</sup> However, to the best of our knowledge, this structural healing, which is characterized by a decrease of the Raman D-mode of the SWCNTs, is not understood in detail. Herein, we present that highly functionalized SWCNT species may also be destroyed by the thermal treatment under inert gas atmosphere (Scheme 3). This observation is supported by the results of Karousis et al., who also observed a decomposition of the CNT framework during annealing.<sup>85</sup> To investigate the influence of the elevated temperatures, most conveniently, the carboxylated SWCNT derivative SWCNT(COOH)<sub>n</sub> (THF, ultrasound) (3) ( $A_D/A_G = 5.1–633$  nm) after TGA-MS analysis was subjected to Raman spectroscopic characterization, absorption spectroscopy, and AFM.

The thermal treatment of SWCNT(COOH)<sub>n</sub> (THF/ultrasound) (3) under inert gas atmosphere (He), heating from room temperature to 100 °C (1 h steady temperature), 100–700 °C (10 °C/min), at 700 °C 1 h steady temperature, yields a carbon-based material TGA-SWCNT(COOH)<sub>n</sub> (THF/ultrasound) (12), with a Raman spectrum (633 nm excitation wavelength)

as shown in Figure 7 (for 532 and 785 nm, see Figures S21 and S22, respectively). Obviously, this thermally processed material does only exhibit a partially reduced D-band intensity (Figure 7a,b) due to the removal of the covalently bound functional entities (see TGA-MS discussion). In addition, the RBM region of TGA-SWCNT(COOH)<sub>n</sub> (THF/ultrasound) (12) (Figure 6c) does not reflect the characteristic signal distribution as observed in the as-received starting material. On the contrary, the metallic RBM signals after the thermal treatment are even more pronounced in comparison to the functionalized derivative SWCNT(COOH)<sub>n</sub> (THF/ultrasound) (3), whereas the semiconducting RBM signals have completely vanished except for the very faint remaining signal of the originally very intensive (9,4) mode. This discovery leads to the conclusion that the highly functionalized semiconducting and small metallic SWCNTs are degraded during the thermal process due to their decreased thermal stability in comparison to comparatively little functionalized SWCNT species. As a consequence, a sample mainly containing unfunctionalized, metallic nanotubes can be obtained by this way.

The selective degradation in contrast to the expected thermal defunctionalization of the highly functionalized SWCNT species is further substantiated by an in-depth resonant Raman-RBM analysis. In the corresponding RBM plot (Figure 8) where the excitation energy has been tuned in the range from 579 to 613 nm, the characteristic metallic resonance signals are detected after the thermal annealing process, whereas virtually no signal is observed for the semiconducting tubes (except for traces of the (9,4) SWCNT).

This destruction of the highly functionalized SWCNTs is further supported by absorption spectroscopy, as the material after thermal treatment redispersed in an aqueous surfactant solution (2 wt % SDC) is characterized by the absence of peaks associated with semiconducting nanotubes (Figure 7d) as is most clearly discernible in comparison to the as-received SWCNT starting material. It is worth noticing that the non resonant background<sup>86</sup> in the absorption spectrum is significantly increased as compared to the reference spectrum, which may be attributed to (i) a lack of debundling in the sample or (ii) the presence of amorphous carbon.

To shed light into this question, the sample was subjected to atomic force microscopy after spin-casting the dispersion on Si/SiO<sub>2</sub> wafers (300 nm oxide layer thickness). The representative images displayed in Figure S23 (Supporting Information) reveal that the nanotubes are well dispersed in the aqueous surfactant solution and that they are furthermore of high structural perfection. Additionally, particles with heights of 10–20 nm are

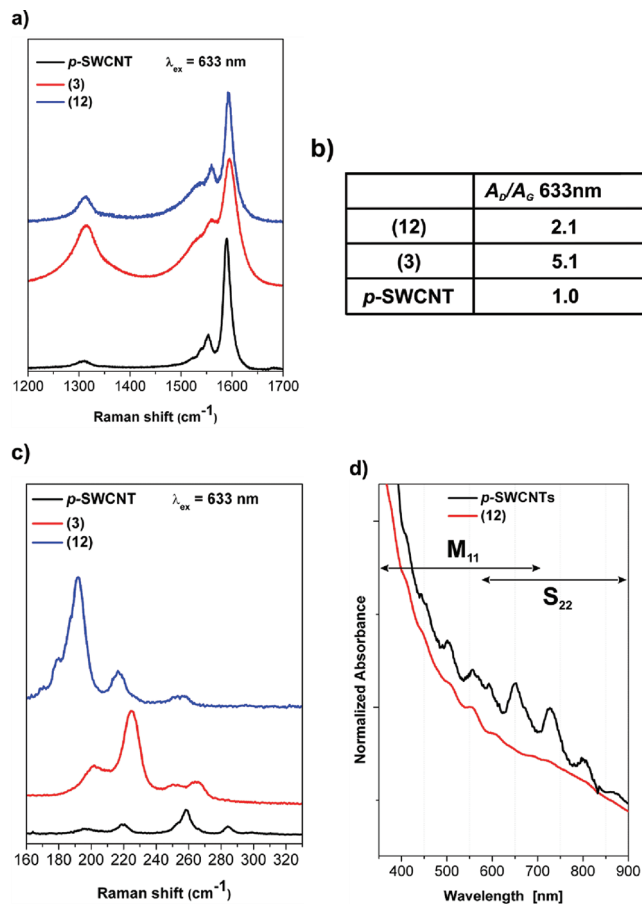


**Figure 7.** (a) Raman D- and G-modes, (b) values of the respective  $A_D/A_G$  intensities, and (c) RBM spectra of the as-received starting material (p-SWCNT), the sidewall carboxylated SWCNT material (SWCNT(COOH)<sub>n</sub> (THF/ultrasound) (3)), and the thermally treated material (TGA-SWCNT(COOH)<sub>n</sub> (THF/ultrasound) (12)) at 633 nm excitation wavelength. (d) Optical absorption spectra of TGA-SWCNT(COOH)<sub>n</sub> (THF/ultrasound) (12) (sidewall carboxylated SWCNTs after thermal treatment under inert gas atmosphere) as compared to the as-received SWCNT starting material. In both cases, the solid material was dispersed in aqueous surfactant solution (2 wt % SDC) by sonication, and the supernatant after centrifugation was analyzed. The spectra were normalized to 825 nm.

observed, which can be traced back to amorphous carbon that has been generated by the annealing procedure. Accordingly, we propose that the highly functionalized SWCNTs could not be defunctionalized by the thermal treatment under inert gas atmosphere, but that they were completely destroyed yielding amorphous material. This is fully consistent with the obtained Raman data, where only a partial reduction of the defect induced D-mode is observed.

This thermal degradation of highly functionalized SWCNTs is not a functional group specific process as the same behavior is also observed for highly functionalized perfluorobutyl alkylated SWCNTs. Herein, thermal annealing of SWCNT(PFBI)<sub>n</sub> (THF/ultrasound) (8) does also lead to a degradation of highly functionalized semiconducting SWCNTs and to a structural annealing of the little functionalized metallic species. The respective Raman data of TGA-SWCNT(PFBI)<sub>n</sub> (THF/ultrasound) (13) can be found in the Supporting Information (Figure S24). Therefore, we postulate that there has to be a threshold

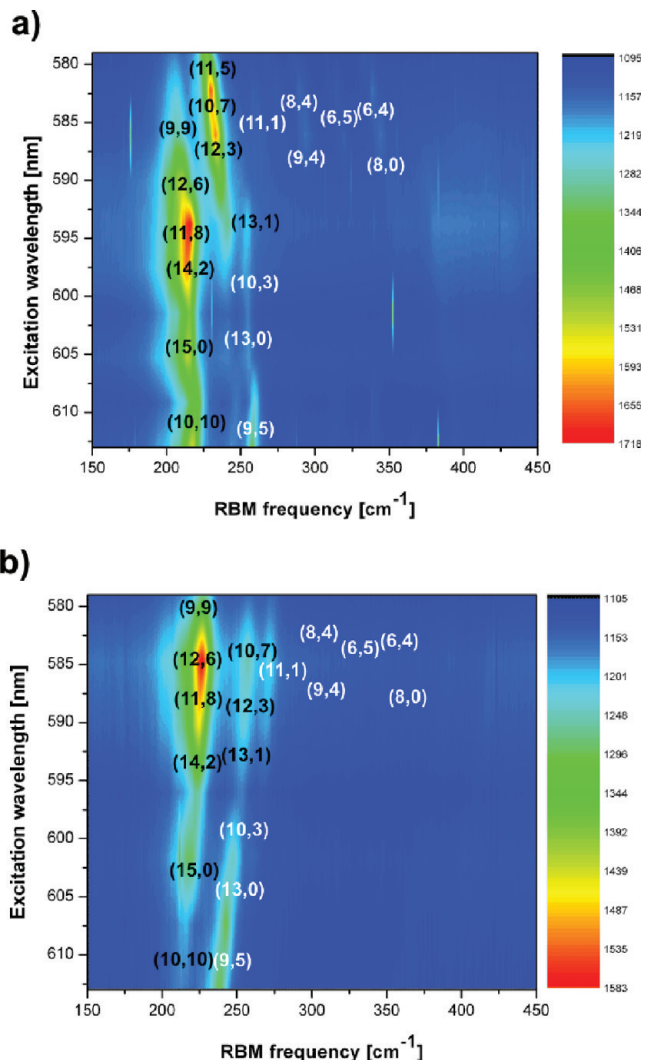


**Figure 8.** Raman RBM plots of (a) as-received HiPCO SWCNTs and (b) TGA-SWCNT(COOH)<sub>n</sub> (THF/ultrasound) (12). Fourteen spectra have been acquired in the excitation range between 579 and 613 (8 nm spacing). Metallic  $(n,m)$ -indices colored in black, semiconducting  $(n,m)$ -indices colored in white. The observed blue-shift of the RBM intensity values after the TGA treatment is caused by a distinct bundling due to the defunctionalization.

level for the  $\text{sp}^3$ -defect density in the SWCNT carbon lattice. Up to this point, a high temperature annealing process does indeed lead to a detachment of the covalently bound addend and to a restoration of the intact  $\text{sp}^2$ -framework. However, above this threshold, the reversibility of the sidewall addition by thermal annealing is no longer ensured for highly functionalized material, and the elevated temperatures lead to a progressive destruction of the nanotube scaffold and to the generation of amorphous carbon.

## CONCLUSIONS

The study presented here constitutes a fundamental breakthrough in covalent nanotube chemistry, as by the highly innovative functionalization sequence, sidewall polycarboxylated nanotubes are accessible where the structural integrity of the  $\sigma$ -carbon framework remains intact in contrast to classical oxidation. From a chemist's point of view, this is highly appealing, as

the carboxylic acid functionalities are the ideal anchor group for further derivatization reactions, as has exemplarily been shown by the coupling reactions within this article. This will drive the field of nanotube science significantly forward, as the surface properties of the nanotubes can be tailored according to the needs. In this regard, it is extremely versatile that the degree of functionalization can be tuned by external stimuli such as pressure.

In addition, the development of novel reaction conditions for the electrophilic attack of charged SWCNT intermediates opened the door for the very pronounced selective sidewall derivatization of semiconducting nanotubes, never observed before. Obviously, the underlying selectivity is not very dependent on the nature of the electrophilic addend. The tunable functionalization degrees are also chameleonic with respect to the investigation of the selectivity as the detailed analysis of varying functionalization degrees enabled one to demonstrate that the small diameter semiconducting SWCNTs are derivatized first, followed by larger diameter semiconducting and concomitantly small diameter metallic species. Large diameter metallic nanotubes have been recovered unharmed in any case, as has strikingly been shown by an in-depth analysis of the material after the separation according to structural integrity by density gradient ultracentrifugation.

Because of the high accessible functionalization degrees in combination with the selective nature of the functionalization sequence, a novel separation approach was unveiled on the basis of the thermal degradation of functionalized nanotubes. In principle, the thermal annealing under inert gas can be used to yield metallic SWCNTs of a desired diameter range (due to the varying functionalization degrees that are accessible) in their pristine form. Similar scenarios have previously been described as constructive destruction.<sup>87,88</sup> However, up to now, the selective breakdown only of metallic SWCNTs has been achieved yielding the semiconducting counterparts, which is in marked contrast to the results of the study presented here.

We expect that these results will impact a broad field of potential carbon nanotube applications, especially polymer reinforcement or the integration in matrixes in general in the case of the carboxylated nanotubes. Alternatively, the nonfunctionalized metallic SWCNTs that are available by a highly scalable separation scenario will be of interest for conductive coatings, transparent electrodes, and so on.

## ■ EXPERIMENTAL SECTION

**Materials.** Purified HiPCO SWCNTs (grade: pure; lot number P0261, TGA residue 13.3 wt %; and P0355, TGA residue 5 wt %) were purchased from Unidym Inc. (Sunnyvale, CA). All SWCNTs were used without further treatment prior to the functionalization. Chemicals and solvents were purchased from Sigma Aldrich Co. (Germany) and Acros Organics (Belgium, Part of Fisher Scientific) and used as-received. THF was distilled over sodium metal. NH<sub>3</sub> was obtained by Riesner-Gase GmbH + Co KG (Germany), purity 5.0, and CO<sub>2</sub> was from Westfalen AG (Germany), purity 4.5.

**SWCNT(COOH)<sub>n</sub> (Birch) (1) (Common Birch Reduction).** A heat-dried and argon-purged four-necked round-bottomed flask (250 mL) equipped with two gas inlets and pressure compensation was cooled to -78 °C (acetone/dry ice), and ammonia (100 mL) was condensed. HiPCO SWCNTs (P0355) (10 mg, 0.83 mmol of carbon) were dispersed in the liquid ammonia, and 5 equiv of sodium metal, related to moles of carbon (0.10 mg, 4.16 mmol), was added and stirred

for 1 h, yielding a blue-black colored, stable dispersion. Subsequently, carbon dioxide was passed into the solution for 1 h (0.5 bar) accompanied by the formation of a white precipitate. Afterward, the respective Birch conditions were re-established by the addition of sodium metal, followed by an additional application of gaseous CO<sub>2</sub>. This procedure was repeated for four further cycles. Finally, the cooling was removed, and the solution was kept stirring until the complete evaporation of ammonia. The residue was dissolved in water/THF (each 100 mL), and the reaction byproducts were removed by aqueous extraction with cyclohexane (100 mL) in a separation funnel. The water/THF phase was discarded, and the cyclohexane layer with the functionalized nanotubes was purged two times with water and THF (100 mL, each). The organic layer with the functionalized nanotubes was filtered through a 0.2 μm reinforced cellulose membrane filter (Sartorius) and thoroughly washed with THF, iso-propanol, ethanol, and water, 250 mL each. The resulting black solid was dried in a vacuum oven at 75 °C overnight.

**SWCNT(COOH)<sub>n</sub> (THF) (2) (Modified Birch Reduction).** In a heat-dried and argon-purged four-necked round-bottomed flask (250 mL) equipped with two gas inlets and pressure compensation, HiPCO SWCNTs (P0355) (10 mg, 0.83 mmol of carbon) were dispersed in 100 mL of anhydrous THF under 30 min ultrasonication. The flask with the dispersion was cooled to -78 °C (acetone/dry ice), and ammonia (100 mL) was condensed. After the addition of lithium metal (29.17 mg, 4.16 mmol), the system was stirred for 1 h, yielding a blue-black colored, stable dispersion. The cooling was removed, and the solution was kept stirring until the complete evaporation of the ammonia. The resulting lithium-bronze was removed by a syringe. Subsequently, carbon dioxide was bubbled through the solution (0.5 bar) for 1 h. Afterward, in a separation funnel, water (100 mL) and cyclohexane (100 mL) were added to the THF dispersion. The water/THF phase was discarded, and the cyclohexane layer with the functionalized nanotubes was purged two times with water and THF (100 mL, each). The organic layer with the nanotubes was filtered through a 0.2 μm reinforced cellulose membrane filter (Sartorius) and thoroughly washed with THF, iso-propanol, ethanol, and water, 250 mL each. The resulting black solid was dried in a vacuum oven at 75 °C overnight.

**SWCNT(COOH)<sub>n</sub> (THF/Ultrasonic) (3) HiPCO Batch P0355, (4) HiPCO batch P0261.** Nanotube functionalization and workup was carried out analogously to the procedure described for 2. After the evaporation of the ammonia and the removal of the lithium bronze, the THF solution was ultrasonicated for 30 min prior to the addition of CO<sub>2</sub>.

**SWCNT(COOH)<sub>n</sub> (THF/Ultrasonic/30 bar) (5) 30 bar and SWCNT(COOH)<sub>n</sub> (THF/Ultrasonic/55 bar) (6) 55 bar.** In a heat-dried and argon-purged four-necked round-bottomed flask (250 mL) equipped with two gas inlets and pressure compensation, HiPCO SWCNTs (P0261) (10 mg, 0.83 mmol of carbon) were dispersed in 100 mL of anhydrous THF under 30 min ultrasonication. The flask with the dispersion was cooled to -78 °C (acetone/dry ice), and ammonia (100 mL) was condensed. After the addition of lithium metal (29.17 mg, 4.16 mmol), the system was stirred for 1 h, yielding a blue-black colored, stable dispersion. The cooling was removed, and the solution was kept stirring until the complete evaporation of the ammonia. The resulting lithium-bronze was removed by a syringe, and the THF solution was ultrasonicated for 30 min prior to the addition of CO<sub>2</sub>. The system was transferred into an autoclave reactor, which was subsequently sealed. The THF solution was stirred by a magnetic stirring bar, and CO<sub>2</sub> was applied to the reactor through a pressure valve (30 and 55 bar, respectively) and kept stirring under constant pressure for 1 h. Afterward, the pressure was slowly lowered to atmospheric conditions. The workup of the functionalized material was carried out analogously to the procedure described for 2.

**SWCNT(PFB)<sub>n</sub> (THF) (7).** In a heat-dried and argon-purged four-necked round-bottomed flask (250 mL) equipped with two gas inlets

and pressure compensation, HiPCO SWCNTs (P0355) (10 mg, 0.83 mmol of carbon) were dispersed in 100 mL of anhydrous THF by 30 min ultrasonication. The flask with the dispersion was cooled to  $-78^{\circ}\text{C}$  (acetone/dry ice), and ammonia (100 mL) was condensed. After the addition of lithium (29.17 mg, 4.16 mmol), the SWCNTs and the dissolved lithium were stirred for 1 h in the blue-black stable dispersion. The cooling was removed, and the solution was kept stirring until the complete evaporation of the ammonia. The resulting lithium-bronze was removed by a syringe. Subsequently, 1.44 mL of perfluorobutyl iodide (8.32 mmol) was added dropwise over a period of 10 min. The workup of the functionalized material was carried out analogously to the procedure described for 2.

**SWCNT(PFBI)<sub>n</sub> (THF/Ultrasound) (8).** Nanotube functionalization and workup were carried out analogously to the procedure described for 7. After the evaporation of the ammonia and the removal of the lithium-bronze, the THF solution was ultrasonicated for 30 min prior to the addition of PFBI.

**SWCNT(COO-ferrocenylmethyl)<sub>n</sub> (9), SWCNT(COO-thiophenylmethyl)<sub>n</sub> (10), and SWCNT(COO-ethylpyridinium bromide)<sub>n</sub> (11).** In a heat-dried and argon-purged round-bottomed flask (250 mL) equipped with two gas inlets and pressure compensation, CO<sub>2</sub>-SWCNTs (8 mg, 0.67 mmol of carbon) were dispersed in 100 mL of anhydrous THF by 30 min ultrasonication. Subsequently, 0.75 equiv of the ferrocenemethanol (108 mg, 0.5 mmol), 2-thiophenemethanol (0.06 mL, 0.5 mmol), and *N*-(hydroxyethyl)pyridinium bromide<sup>78</sup> (130 mg, 0.5 mmol) were added, respectively. In a following step, 1.3 equiv of dicyclohexylcarbodiimide DCC (0.65 mmol, 135 mg) and 0.4 equiv of 4-(dimethylamino)-pyridine DMAP (0.2 mmol, 25 mg) were added. The dispersion was stirred for 96 h, and afterward the reaction was transferred to a separation funnel with cyclohexane and water (each 100 mL). The water/THF phase was discarded, and the cyclohexane layer with the functionalized nanotubes was purged two times with water and THF (100 mL, each). The organic layer with the functionalized nanotubes was filtered through a 0.2  $\mu\text{m}$  reinforced cellulose membrane filter (Sartorius) and thoroughly washed with THF, iso-propanol, ethanol, and water, 700 mL each. The resulting black solid was dried in a vacuum oven at  $75^{\circ}\text{C}$  overnight.

## ■ INSTRUMENTS AND MEASUREMENTS

**Raman Spectroscopy.** Raman spectroscopic characterization was carried out on a Horiba Jobin Yvon LabRAM Aramis confocal Raman microscope (excitation wavelengths: 532, 633, and 785 nm) with a laser spot size of  $\sim 1 \mu\text{m}$  (Olympus LMPPlanFl 100 $\times$ , NA 0.80). The incident laser power was kept as low as possible to avoid structural sample damage: 240  $\mu\text{W}$  (532 nm), 114  $\mu\text{W}$  (622 nm), 3 mW (785 nm). Multiple Raman spectra (five) were obtained from different spots of the buckypapers and averaged.

The resonant Raman measurements were carried out using a micro-Raman setup in backscattering geometry, the samples being excited by a tunable laser with about 0.4 mW laser power on the samples. A charge-coupled device is used to detect the signal after analyzing the signal via a triple monochromator. The spectrometer was calibrated in frequency using a Neon lamp. Bulk CaF<sub>2</sub> was used to normalize the intensities of the RBM signal at different excitation energies.

**Thermogravimetric Analysis combined with Mass Spectrometry (TGA-MS).** Thermogravimetric analysis (TGA) equipped with a mass spectrometer (MS) was performed on a Netzsch STA 409 CD instrument equipped with a Skimmer QMS 422 mass spectrometer (MS/EI) with the following programmed time-dependent temperature profile: 24–100 °C with 10 K/min gradient, isothermal stabilization for 1 h, 100–700 °C with 10 K/min gradient, isothermal stabilization for 1 h and cooling to 24 °C. The initial sample weights were about 5–10 mg, and the whole experiment was executed under inert gas atmosphere with

a He gas flow of 80 mL/min. TGA treatment of SWCNT(COOH)<sub>n</sub> (THF/ultrasound) (3) yields defunctionalized TGA-SWCNT(COOH)<sub>n</sub> (THF/ultrasound) (12), and the TGA treatment of PFBI functionalized derivative SWCNT(PFBI)<sub>n</sub> (THF/ultrasound) (8) yields TGA-SWCNT(PFBI)<sub>n</sub> (THF/ultrasound) (13) in analogy.

**Absorption Spectroscopy.** UV-vis (400–900 nm) and nIR (900–1400 nm) absorption spectra were recorded on a Perkin-Elmer Lambda 1050 in transmission with 1 cm path length in quartz glass suprasil (Hellma) cuvettes. In the case of the aqueous detergent solution, the background of H<sub>2</sub>O was subtracted. Prior to dispersing the SWCNTs, the material was homogenized by pregrinding with pestle and mortar. Dispersions were prepared by ultrasonicating the SWCNTs with initial concentrations of 0.1 g L<sup>-1</sup> in the respective solvents in a bath type sonicator for 20 min. For all dispersion experiments, the nanotubes were sonicated in vials of the same shape and size with an approximately equal volume of solvent that was placed at the same position in the sonic bath with temperatures not exceeding 27 °C and equal filling level of the sonic bath. The homogeneous mixture was then centrifuged in a Sigma 4K15. Unless otherwise noted, the supernatant after 20 min centrifugation at 15 k rpm was decanted and subjected to further analysis. The SWCNT concentration after centrifugation in NMP was determined from the absorption coefficient at 660 nm of HiPCO SWCNTs in NMP (3260 L g<sup>-1</sup> m<sup>-1</sup>).<sup>11</sup> In the case of the THF dispersions, the wet SWCNTs after the filtration procedure were immediately immersed in THF without drying to avoid unwanted aggregation. The SWCNT concentration in those samples (prior to and after centrifugation) was determined gravimetrically.

**Fluorescence Spectroscopy.** The SWCNT nIR emission was recorded from aqueous surfactant solution (2 wt % sodium deoxycholate, preparation in analogy to absorption spectroscopy samples) with a Nanospectralyzer NS1 from Applied Nanofluorescence with laser excitations of 660 and 785 nm. Integration times were 300 ms, and 50 spectra were averaged. In all cases, the SWCNT dispersions were diluted to absorbance intensities of 0.04 per 1 cm path length at 660 nm.

**Infrared Spectroscopy.** IR spectra were obtained in transmission with KBr as matrix on a Tensor 27 (Bruker). The SWCNTs were preground with pestle and mortar prior to homogeneously distribute 0.1 wt % of functionalized SWCNTs with KBr by ball milling. Pellets were fabricated by pressing the KBr under vacuum at 10 tons for 10 min. 1000 scans with a resolution of 4 cm<sup>-1</sup> have been recorded with a KBr pellet of equal thickness as background.

**Atomic Force Microscopy.** AFM tapping mode images of the spin-casted dispersions (100 rps on Si/SiO<sub>2</sub> wafers) were recorded on a Solver Pro scanning probe microscope (NT-MDT) equipped with a Sony Exwave HAD camera optical zoom (6.5).

**Zeta Potential Analysis.** Zeta potential measurements were carried out on a Malvern Zetasizer Nano system with irradiation from a 633 nm He–Ne laser. The samples were injected in folded capillary cells, and the electrophoretic mobility ( $\mu$ ) was measured using a combination of electrophoresis and laser Doppler velocimetry techniques. The electrophoretic mobility relates the drift velocity of a colloid ( $v$ ) to the applied electric field ( $E$ ):  $v = \mu E$ . All measurements were conducted at 25 °C. The zeta potential  $\zeta$  is related to the measured electrophoretic mobility  $\mu$  according to the Smoluchowski approximation. The pH titration was carried out by the aid of a MPT2 autotitrator that increased the pH in steps of 0.5 by the addition of the appropriate amount of 0.1 M NaOH. At each addition step, the zeta potential was recorded three times. The data points in the zeta potential versus pH plot constitute the average of two independent titrations of the highly functionalized SWCNTs. Prior to the pH titration, the functionalized SWCNTs were immersed in water, and the pH was adjusted to 2 by the addition of HCl.

**Density Gradient Ultracentrifugation.** Density gradients were formed from aqueous solutions of the nonionic density gradient iodixanol (purchased as Optiprep 60 wt % in water, 1.32 g cm<sup>-3</sup>). The linear density gradients were created directly in the centrifuge vial

(Beckman Polyclear, 5 mL volume) by layering and subsequent diffusion of five discrete layers with decreasing iodixanol concentration from bottom to top of 60 wt % (0.7 mL), 40 wt % (1.5 mL), 32.5 wt % (1 mL; layer containing SWCNTs), 30 wt % (1 mL), and 20 wt % (0.8 mL), respectively. Sodium deoxycholate (SDC) was used as surfactant for the stabilization of the nanotubes with a concentration of 2 wt % throughout the centrifugation vial. For the preparation of the layer containing the nanotube material, 0.5 g L<sup>-1</sup> SWCNTs were dispersed in 2 wt % SDC solutions by sonication (30 min in a bath type sonicator). After mild precentrifugation (15 k rpm, Sigma 4K15, 30 min), the appropriate amount of iodixanol was added to the supernatant dispersions to yield concentrations of 32.5 wt %. The mixture was then directly used as a layer in the gradient. The ultracentrifugation experiment was carried out in a swinging bucket rotor (MLS-50) at 40 k rpm for 17.5 h. The nonfunctionalized SWCNT material traveled upward during the centrifugation, while the bundles sedimented to the very bottom.

Ultrasonication was performed with a Branson 2510-DTH Ultrasonic Processor (42 kHz, 239 W).

## ■ ASSOCIATED CONTENT

**S Supporting Information.** Detailed characterization of functionalized SWCNTs by Raman spectroscopy, absorption spectroscopy, atomic force microscopy, IR spectroscopy, zeta potential, and thermogravimetric analysis coupled to mass spectrometry. Details on the coupling reactions, density gradient ultracentrifugation, as well as selective constructive destruction by thermal annealing. This material is available free of charge via the Internet at <http://pubs.acs.org>.

## ■ AUTHOR INFORMATION

### Corresponding Author

andreas.hirsch@chemie.uni-erlangen.de

## ■ ACKNOWLEDGMENT

This work was supported by the Deutsche Forschungsgemeinschaft (DFG) and the Cluster of Excellence “Engineering of Advanced Materials” (EAM). We thank the Interdisciplinary Center for Molecular Materials (ICMM) for financial support and Torsten Schunk for the synthesis of the N-(hydroxyethyl)pyridinium bromide. The TUB authors acknowledge partial support by the DFG through Cluster of Excellence “UniCat”. J.M. acknowledges support by ERC grant no. 259286.

## ■ REFERENCES

- O’Connell, M. J., Ed. *Carbon Nanotubes: Properties and Applications*; CRC Press LLC: Boca Raton, FL, 2006.
- Dresselhaus, M. S.; Dresselhaus, G.; Avouris, P. *Carbon Nanotubes: Synthesis, Structure, Properties, and Applications*; Springer: Berlin, 2001.
- Guldi, D. M.; Martín, N. *Carbon Nanotubes and Related Structures: Synthesis, Characterization, Functionalization, and Applications*; Wiley-VCH: New York, 2010.
- Jorio, A.; Dresselhaus, G.; Dresselhaus, M. S. *Carbon Nanotubes: Advanced Topics in the Synthesis, Structure, Properties and Applications*; Springer: Berlin, 2007.
- Kelly, L.; Meyyappan, M. *Carbon Nanotubes: Science and Applications*; CRC Press Inc.: Boca Raton, FL, 2004.
- Reich, S.; Thomsen, C.; Maultzsch, J. *Carbon Nanotubes: Basic Concepts and Physical Properties*; Wiley-VCH: Weinheim, 2004.
- Hirsch, A. *Angew. Chem., Int. Ed.* **2002**, *41*, 1853.
- Hirsch, A. *Nat. Mater.* **2010**, *9*, 868.
- Bahr, J. L.; Mickelson, E. T.; Bronikowski, M. J.; Smalley, R. E.; Tour, J. M. *Chem. Commun.* **2001**, 193.
- Ausman, K. D.; Piner, R.; Lourie, O.; Ruoff, R. S.; Korobov, M. *J. Phys. Chem. B* **2000**, *104*, 8911.
- Bergin, S. D.; Sun, Z.-Y.; Streich, P.; Hamilton, J.; Coleman, J. N. *J. Phys. Chem. C* **2010**, *114*, 231.
- Coleman, J. N. *Adv. Funct. Mater.* **2009**, *19*, 3680.
- Prato, M.; Kostarelos, K.; Bianco, A. *Acc. Chem. Res.* **2008**, *41*, 60.
- Peng, X.; Wong, S. S. *Adv. Mater.* **2009**, *21*, 625.
- Byrne, M. T.; Gun’ko, Y. K. *Adv. Mater.* **2010**, *22*, 1672.
- Karousis, N.; Tagmatarchis, N.; Tasis, D. *Chem. Rev.* **2010**, *110*, 5366.
- Lu, F.; Meziani, M. J.; Cao, L.; Sun, Y.-P. *Langmuir* **2011**, *27*, 4339.
- Arnold, M. S.; Green, A. A.; Hulvat, J. F.; Stupp, S. I.; Hersam, M. C. *Nat. Nanotechnol.* **2006**, *1*, 60.
- Martel, R. *ACS Nano* **2008**, *2*, 2195.
- Hauke, F.; Hirsch, A. In *Carbon Nanotubes and Related Structures*; Guldi, D. M., Martín, N., Eds.; Wiley-VCH: Weinheim, 2010; p 135.
- Tasis, D.; Tagmatarchis, N.; Bianco, A.; Prato, M. *Chem. Rev.* **2006**, *106*, 1105.
- Graupner, R.; Hauke, F. In *The Oxford Handbook of Nanoscience and Technology*; Narlikar, A. V., Fu, Y. Y., Eds.; Oxford University Press: New York, 2010; Vol. I: Basic Aspects, p 508.
- Hirsch, A.; Vostrowsky, O. *Top. Curr. Chem.* **2005**, *245*, 193.
- Liu, J.; Rinzler, A. G.; Dai, H.; Hafner, J. H.; Bradley, R. K.; Boul, P. J.; Lu, A.; Iverson, T.; Shelimov, K.; Huffman, C. B.; Rodriguez-Macias, F.; Shon, Y.-S.; Lee, T. R.; Colbert, D. T.; Smalley, R. E. *Science* **1998**, *280*, 1253.
- Hirsch, A.; Vostrowsky, O. *Functionalization of Carbon Nanotubes*; Wiley-VCH Verlag: Weinheim, 2007.
- Ford, W. E.; Jung, A.; Hirsch, A.; Graupner, R.; Scholz, F.; Yasuda, A.; Wessels, J. M. *Adv. Mater.* **2006**, *18*, 1193.
- Chen, S.; Shen, W.; Wu, G.; Chen, D.; Jiang, M. *Chem. Phys. Lett.* **2005**, *402*, 312.
- Peng, H.; Alemany, L. B.; Margrave, J. L.; Khabashesku, V. N. *J. Am. Chem. Soc.* **2003**, *125*, 15174.
- Chattopadhyay, J.; de Cortez, F.; Chakraborty, S.; Slater, N. K. H.; Billups, W. E. *Chem. Mater.* **2006**, *18*, 5864.
- Strano, M. S.; Dyke, C. A.; Usrey, M. L.; Barone, P. W.; Allen, M. J.; Shan, H.; Kittrell, C.; Hauge, R. H.; Tour, J. M.; Smalley, R. E. *Science* **2003**, *301*, 1519.
- Doyle, C. D.; Rocha, J.-D. R.; Weisman, R. B.; Tour, J. M. *J. Am. Chem. Soc.* **2008**, *130*, 6795.
- Schmidt, G.; Filoromo, A.; Derycke, V.; Bourgoin, J.-P.; Chenevier, P. *Chem.-Eur. J.* **2011**, *17*, 1415.
- Wunderlich, D.; Hauke, F.; Hirsch, A. *J. Mater. Chem.* **2008**, *18*, 1493.
- Graupner, R.; Abraham, J.; Wunderlich, D.; Vencelova, A.; Lauffer, P.; Roehrl, J.; Hundhausen, M.; Ley, L.; Hirsch, A. *J. Am. Chem. Soc.* **2006**, *128*, 6683.
- Wunderlich, D.; Hauke, F.; Hirsch, A. *Chem.-Eur. J.* **2008**, *14*, 1607.
- Luente-Schultz, R. M.; Moore, V. C.; Leonard, A. D.; Price, B. K.; Kosynkin, D. V.; Lu, M.; Partha, R.; Conyers, J. L.; Tour, J. M. *J. Am. Chem. Soc.* **2009**, *131*, 3934.
- Wu, W.; Li, R.; Bian, X.; Zhu, Z.; Ding, D.; Li, X.; Jia, Z.; Jiang, X.; Hu, Y. *ACS Nano* **2009**, *3*, 2740.
- Niu, L.; Li, P.; Chen, Y.; Wang, J.; Zhang, J.; Zhang, B.; Blau, W. J. *J. Polym. Sci., Part A: Polym. Chem.* **2011**, *49*, 101.
- Homenick, C. M.; Sheardown, H.; Adronov, A. *J. Mater. Chem.* **2010**, *20*, 2887.
- Liang, F.; Sadana, A. K.; Peera, A.; Chattopadhyay, J.; Gu, Z.; Hauge, R. H.; Billups, W. E. *Nano Lett.* **2004**, *4*, 1257.
- Chattopadhyay, J.; Sadana, A. K.; Liang, F.; Beach, J. M.; Xiao, Y.; Hauge, R. H.; Billups, W. E. *Org. Lett.* **2005**, *7*, 4067.
- Billups, W. E.; Liang, F.; Chattopadhyay, J.; Beach, J. M. *ECS Trans.* **2007**, *2*, 65.

- (43) Gebhardt, B.; Syrgiannis, Z.; Backes, C.; Graupner, R.; Hauke, F.; Hirsch, A. *J. Am. Chem. Soc.* **2011**, *133*, 7985.
- (44) Chattopadhyay, J.; Chakraborty, S.; Mukherjee, A.; Wang, R.; Engel, P. S.; Billups, W. E. *J. Phys. Chem. C* **2007**, *111*, 17928.
- (45) Mukherjee, A.; Combs, R.; Chattopadhyay, J.; Abmayr, D. W.; Engel, P. S.; Billups, W. E. *Chem. Mater.* **2008**, *20*, 7339.
- (46) Mueller, M.; Maultzsch, J.; Wunderlich, D.; Hirsch, A.; Thomsen, C. *Phys. Status Solidi RRL* **2007**, *1*, 144.
- (47) Thomsen, C.; Reich, S. *Top. Appl. Phys.* **2007**, *108*, 115.
- (48) Graupner, R. *J. Raman Spectrosc.* **2007**, *38*, 673.
- (49) Mueller, M.; Maultzsch, J.; Wunderlich, D.; Hirsch, A.; Thomsen, C. *Phys. Status Solidi B* **2007**, *244*, 4056.
- (50) Gebhardt, B.; Graupner, R.; Hauke, F.; Hirsch, A. *Eur. J. Org. Chem.* **2010**, 1494.
- (51) Syrgiannis, Z.; Gebhardt, B.; Dotzer, C.; Hauke, F.; Graupner, R.; Hirsch, A. *Angew. Chem., Int. Ed.* **2010**, *49*, 3322.
- (52) Jorio, A.; Araujo, P. T.; Doorn, S. K.; Maruyama, S.; Chacham, H.; Pimenta, M. A. *Phys. Status Solidi B* **2006**, *243*, 3117.
- (53) Maultzsch, J.; Telg, H.; Reich, S.; Thomsen, C. *Phys. Rev. B* **2005**, *72*, 205438/1.
- (54) Ericson, L. M.; Pehrsson, P. E. *J. Phys. Chem. B* **2005**, *109*, 20276.
- (55) Reich, S.; Thomsen, C.; Ordejon, P. *Phys. Rev. B* **2002**, *65*, 155411/1.
- (56) Heller, D. A.; Barone, P. W.; Swanson, J. P.; Mayrhofer, R. M.; Strano, M. S. *J. Phys. Chem. B* **2004**, *108*, 6905.
- (57) Miyata, Y.; Maniwa, Y.; Kataura, H. *J. Phys. Chem. B* **2006**, *110*, 25.
- (58) Lu, J.; Lai, L.; Luo, G.; Zhou, J.; Qin, R.; Wang, D.; Wang, L.; Mei, W. N.; Li, G.; Gao, Z.; Nagase, S.; Maeda, Y.; Akasaka, T.; Yu, D. *Small* **2007**, *3*, 1566.
- (59) Paolucci, D.; Franco, M. M.; Iurlo, M.; Marcaccio, M.; Prato, M.; Zerbetto, F.; Penicaud, A.; Paolucci, F. *J. Am. Chem. Soc.* **2008**, *130*, 7393.
- (60) Voiry, D.; Roubeau, O.; Penicaud, A. *J. Mater. Chem.* **2010**, *20*, 4385.
- (61) Furtado, C. A.; Kim, U. J.; Gutierrez, H. R.; Pan, L.; Dickey, E. C.; Eklund, P. C. *J. Am. Chem. Soc.* **2004**, *126*, 6095.
- (62) Giordani, S.; Bergin, S.; Nicolosi, V.; Lebedkin, S.; Blau, W. J.; Coleman, J. N. *Phys. Status Solidi B* **2006**, *243*, 3058.
- (63) Giordani, S.; Bergin, S. D.; Nicolosi, V.; Lebedkin, S.; Kappes, M. M.; Blau, W. J.; Coleman, J. N. *J. Phys. Chem. B* **2006**, *110*, 15708.
- (64) Bergin, S. D.; Nicolosi, V.; Streich, P. V.; Giordani, S.; Sun, Z.; Windle, A. H.; Ryan, P.; Niraj, N. P. P.; Wang, Z.-T. T.; Carpenter, L.; Blau, W. J.; Boland, J. J.; Hamilton, J. P.; Coleman, J. N. *Adv. Mater.* **2008**, *20*, 1876.
- (65) Amiran, J.; Nicolosi, V.; Bergin, S. D.; Khan, U.; Lyons, P. E.; Coleman, J. N. *J. Phys. Chem. C* **2008**, *112*, 3519.
- (66) Wang, F.; Dukovic, G.; Brus, L. E.; Heinz, T. F. *Science* **2005**, *308*, 838.
- (67) Deslippe, J.; Spataru, C. D.; Prendergast, D.; Louie, S. G. *Nano Lett.* **2007**, *7*, 1626.
- (68) Strano, M. S.; Huffman, C. B.; Moore, V. C.; O'Connell, M. J.; Haroz, E. H.; Hubbard, J.; Miller, M.; Rialon, K.; Kittrell, C.; Ramesh, S.; Hauge, R. H.; Smalley, R. E. *J. Phys. Chem. B* **2003**, *107*, 6979.
- (69) Charlier, J. *C. Acc. Chem. Res.* **2002**, *35*, 1063.
- (70) Hu, H.; Zhao, B.; Hamon, M. A.; Kamaras, K.; Itkis, M. E.; Haddon, R. C. *J. Am. Chem. Soc.* **2003**, *125*, 14893.
- (71) Chen, J.; Hamon, M. A.; Hu, H.; Chen, Y.; Rao, A. M.; Eklund, P. C.; Haddon, R. C. *Science* **1998**, *282*, 95.
- (72) O'Connell, M. J.; Bachilo, S. M.; Huffman, C. B.; Moore, V. C.; Strano, M. S.; Haroz, E. H.; Rialon, K. L.; Boul, P. J.; Noon, W. H.; Kittrell, C.; Ma, J.; Hauge, R. H.; Weisman, R. B.; Smalley, R. E. *Science* **2002**, *297*, 593.
- (73) Bachilo, S. M.; Strano, M. S.; Kittrell, C.; Hauge, R. H.; Smalley, R. E.; Weisman, R. B. *Science* **2002**, *298*, 2361.
- (74) Weisman, R. B.; Bachilo, S. M.; Tsypbolski, D. *Appl. Phys. A: Mater. Sci. Process.* **2004**, *78*, 1111.
- (75) Dukovic, G.; White, B. E.; Zhou, Z.; Wang, F.; Jockusch, S.; Steigerwald, M. L.; Heinz, T. F.; Friesner, R. A.; Turro, N. J.; Brus, L. E. *J. Am. Chem. Soc.* **2004**, *126*, 15269.
- (76) Cognet, L.; Tsypbolski, D. A.; Rocha, J.-D. R.; Doyle, C. D.; Tour, J. M.; Weisman, R. B. *Science* **2007**, *316*, 1465.
- (77) Singh, P.; Campidelli, S.; Giordani, S.; Bonifazi, D.; Bianco, A.; Prato, M. *Chem. Soc. Rev.* **2009**, *38*, 2214.
- (78) Rosenlehner, K.; Schunk, T.; Jux, N.; Brettreich, M.; Hirsch, A. *Org. Biomol. Chem.* **2008**, *6*, 2697.
- (79) Kim, W.-J.; Nair, N.; Lee, C. Y.; Strano, M. S. *J. Phys. Chem. C* **2008**, *112*, 7326.
- (80) Backes, C.; Bosch, S.; Mundloch, U.; Hauke, F.; Hirsch, A. *ChemPhysChem* **2011**, *12*, 2576–2580.
- (81) Georgakilas, V.; Vougaris, D.; Vazquez, E.; Prato, M.; Guldi, D. M.; Kukovecz, A.; Kuzmany, H. *J. Am. Chem. Soc.* **2002**, *124*, 14318.
- (82) Sun, Y.-P.; Fu, K.; Lin, Y.; Huang, W. *Acc. Chem. Res.* **2002**, *35*, 1096.
- (83) Lin, Y.; Hill, D. E.; Bentley, J.; Allard, L. F.; Sun, Y.-P. *J. Phys. Chem. B* **2003**, *107*, 10453.
- (84) Dyke, C. A.; Tour, J. M. *Chem.-Eur. J.* **2004**, *10*, 812.
- (85) Karousis, N.; Kobayashi, K.; Shinohara, H.; Tagmatarchis, N. *Small* **2010**, *6*, 2774.
- (86) Itkis, M. E.; Perea, D. E.; Niyogi, S.; Rickard, S. M.; Hamon, M. A.; Hu, H.; Zhao, B.; Haddon, R. C. *Nano Lett.* **2003**, *3*, 309.
- (87) Collins, P. G.; Arnold, M. S.; Avouris, P. *Science* **2001**, *292*, 706.
- (88) Hersam, M. C. *Nat. Nanotechnol.* **2008**, *3*, 387.